CHALMERS
UNIVERSITY OF TECHNOLOGY

Oxidation of UN/U<inf>2</inf>N<inf>3</inf>-UO<inf>2</inf> composites: an evaluation of UO<inf>2</inf> as an oxidation barrier for the nitride

Citation for the original published paper (version of record):
Costa, D., Hedberg, M., Middleburgh, S. et al (2021). Oxidation of UN/U<inf>2</inf>N<inf>3</inf>-UO<inf>2</inf> composites: an evaluation of UO<inf>2</inf> as an oxidation barrier for the nitride phases. Journal of Nuclear Materials, 544.
http://dx.doi.org/10.1016/j.jnucmat.2020.152700

Journal of Nuclear Materials 544 (2021) 152700

Contents lists available at ScienceDirect

Journal of Nuclear Materials

journal homepage: www.elsevier.com/locate/jnucmat

Oxidation of UN/U_2N_3-UO_2 composites: an evaluation of UO_2 as an oxidation barrier for the nitride phases

Diogo Ribeiro Costa[a,b,*], Marcus Hedberg[c], Simon C. Middleburgh[d], Janne Wallenius[a], Pär Olsson[a], Denise Adorno Lopes[b]

[a] KTH Royal Institute of Technology, Nuclear Engineering, 106 91 Stockholm, Sweden
[b] Westinghouse Electric Sweden AB, 721 63 Västerås, Sweden
[c] Chalmers University of Technology, Nuclear Chemistry, 412 96 Göteborg, Sweden
[d] Bangor University, Nuclear Futures Institute, Bangor, Gwynedd, LL57 1UT, UK

ARTICLE INFO

Article history:
Received 15 September 2020
Revised 12 November 2020
Accepted 23 November 2020
Available online 27 November 2020

Keywords:
Accident tolerant fuel
UN-UO_2 composite
oxidation resistance
UN microspheres
UO_2 fuel
α-U_2N_3
thermogravimetric analysis

ABSTRACT

Composite fuels such as UN-UO_2 are being considered to address the lower oxidation resistance of the UN fuel from a safety perspective for use in light water reactors, whilst improving the in-reactor behaviour of the more ubiquitous UO_2 fuel. An innovative UN-UO_2 accident tolerant fuel has recently been fabricated and studied: UN microspheres embedded in UO_2 matrix. In the present study, detailed oxidative thermogravimetric investigations (TGA/DSC) of high-density UN/U_2N_3-UO_2 composite fuels (91-97 %TD), as well as post oxidised microstructures obtained by SEM, are reported and analysed. Triplicate TGA measurements of each specimen were carried out at 5 K/min up to 973 K in a synthetic air atmosphere to assess their oxidation kinetics. The mass variation due to the oxidation reactions (%), the oxidation onset temperatures (OOTs), and the maximum reaction temperatures (MRTs) are also presented and discussed. The results show that all composites have similar post oxidised microstructures with mostly intergranular cracking and spalling. The oxidation resistance of the pellet with initially 10 wt% of UN microspheres is surprisingly better than the UO_2 reference. Moreover, there is no significant difference in the OOT (~557 K) and MRT (~615 K) when 30 wt% or 50 wt% of embedded UN microspheres are used. Therefore, the findings in this article demonstrate that the UO_2 matrix acts as a barrier to improve the oxidation resistance of the nitride phases at the beginning of life conditions.

1. Introduction

After the Fukushima Daiichi disaster in 2011, the nuclear community has strived to engineer a successor to the standard uranium dioxide (UO_2)-Zr fuel-cladding system within light water reactors (LWRs). This severe accident scenario demonstrated that the standard fuel system degrades rapidly in such extreme conditions [1]. From that point on, many studies have been carried out focusing on fabricating accident tolerant fuel (ATF) materials that can withstand accident conditions for a longer time. These new ATF materials have to maintain or enhance the fuel performance under normal and transient operating conditions, as well as during a potential design basis accident (DBA) and beyond-design basis accident (BDBA) [2].

Uranium nitride (UN) has been considered a promising ATF candidate to substitute UO_2 in LWRs mainly because of its higher uranium density, thermal conductivity, and similar melting point in comparison with UO_2 [3]. These improved properties would allow operating the reactor with a lower fuel centreline temperature, which provides the benefit of a higher margin for melting. Additionally, an improved fission density would enable higher burnup, larger power uprates, and longer fuel resident time [4–6] that are often labelled as advanced technology fuel attributes. However, the UN fuel has low oxidation resistance when in contact with the coolant water in the LWR system [7]. In such a situation, the nitride fuel readily reacts with the coolant and loses its structural integrity, resulting in fuel pellet oxidation, pulverisation, washout and relocation.

Composite fuel designs are considered to overcome the lower oxidation resistance of the UN fuel. The main idea of such composites is to combine the UN with a material that has a better oxidation resistance. This material would form a protective barrier

---

[*] Corresponding author.
E-mail address: diogorc@kth.se (D.R. Costa).

https://doi.org/10.1016/j.jnucmat.2020.152700

around the UN and, therefore, prevent its oxidation. Several materials such as CrN and AlN [8], ZrN [9], U_3Si_2 [10,11], and UO_2 [12–14] have been studied. Among these options, UO_2 shows great advantages since it is already used as a fuel in LWR, as well as it has a good oxidation resistance when in contact with the coolant water.

Many studies on UN degradation/oxidation have been performed since the 1960s [7,15-26]. Nevertheless, there are few studies in the literature related to the degradation/oxidation of UN-UO_2 composite fuels [25,27], but none of them is related to UN microspheres embedded in UO2 matrix. Both previous studies used mixtures of UO_2 and UN powders to fabricate the composites. Watkins et al. [25] investigated the degradation behaviour of UN-UO_2 (5-10 wt%) sintered pellets (> 90 %TD) in high-pressure water. The samples were subjected to hydrothermal oxidation in a static autoclave filled with water at high temperatures (523-623 K) and pressures (up to 16.5 MPa), which are relevant to LWR operating conditions for a short duration. The authors concluded that grain boundary attack and spallation are the primary degradation mechanism in hydrothermal oxidation conditions. Shivprasad et al. [27] reported thermogravimetric analyses of UN-UO_2 (5-30 v%) in steam (62-83 %) during heating to 1273 K, and isotherm data for such composites at 623 K under 82 % steam during 12 h. In both thermogravimetric experiments, the addition of UO_2 delayed the oxidation onset temperature when compared to pure UN. So, the autoclave experiments have permitted the reproduction of an LWR-type environment, but have not provided useful information such as the oxidation onset temperature and the maximum reaction rate, as thermogravimetry has provided. Thus, both autoclave and thermogravimetric investigations are relevant and complementary.

An innovative UN-UO_2 accident tolerant fuel has recently been fabricated and studied by the authors of this work [28]: UN microspheres embedded in UO_2 matrix. Since this composite fuel is a new concept, there is no data regarding its oxidation resistance neither using thermogravimetric examination nor autoclave test. As a first approach, thermogravimetric investigations are essential to understand the material parameters which govern the oxidation reactions of this fuel.

In the present study, detailed thermogravimetric (TG) and differential scanning calorimetry (DSC) investigations of the oxidation reactions in a synthetic air atmosphere up to 973 K are reported and discussed. High-density UN-UO_2 (91-97 %TD) composites, within the limits for LWR application [29,30], were selected from our previous study [28] and are investigated here. This work also describes the influence of the amount (wt%) of each phase present in the sintered pellet, i.e. UO_2, UN and α-U_2N_3, on the oxidation kinetics. Additionally, pure $UO_{2.13}$ powder and UN microspheres, as well as UO_2 and UN sintered samples are evaluated and used as references (UO_2 pellet and UN microspheres). As a result of introducing triplicates in the TGA experiments, uncertainties related to the total weight variation (%), oxidation onset temperatures (OOTs), maximum reaction temperatures (MRTs), as well as the reliability of the TG results were obtained and demonstrated. Therefore, from the findings present in this study, future works are encouraged to perform additional investigations to assess the oxidation resistance of this fuel concept in TGA steam oxidation and/or autoclave test in an LWR-type environment.

2. Methods

2.1. UN-UO_2 composite fuel fabrication

Uranium nitride (UN) microspheres were fabricated by the internal sol-gel process at Chalmers University of Technology [31,32]. The reported amounts of nitrogen, carbon and oxygen, as well as the associated errors in the triplicate measurements (given as one standard deviation), were 5.72 ± 0.07 wt%, 833 ± 550 ppm and 1010 ±150 ppm, respectively, which give a chemical formula $U(N_{1.03}C_{0.02}O_{0.02})$. N and O analyses were performed by the inert fusion method, using a LECO TC436DR equipment inside a nitrogen-filled glovebox (< 500 ppm O_2) to minimise oxygen incorporation during sample preparation and analyses. The equipment was calibrated before the analyses by running blank samples for the zero calibration and D-lab standard (provided by Degerfors laboratory) containing 9.71 wt% N and 3 wt% O. The calibration standard was run three times and the furnace constants for N and O, respectively of the instrument, were adjusted if the measurement average deviated from the target value by more than 2 %. C analysis was performed by the combustion method using a LECO CS744 instrument. Prior to carbon measurement, triplicate measurements of blank samples and a calibration standard were performed. The blank samples contained the crucible and combustion accelerator (Lecocell-II, to ensure proper heating of every sample), and the results were used for correcting the measurement baseline to zero. The calibration standard used is a drift standard for calibrating the instrument on top of the multipoint baseline calibration of the instrument. The drift calibration standard used was a carbon-containing steel pin standard from LECO containing 0.799 ± 0.011 wt% C. The as-fabricated UN microspheres were kept under argon for the duration of the investigations (< 1 ppm O_2).

Uranium dioxide (UO_2) powder was provided by Westinghouse Electric Sweden AB, which had the following properties: O/U ratio of 2.13, fill density of 2.19 g/cm^3, specific surface area (B.E.T.) of 5.33 m^2/g, mean particle size of 20.20 µm, and 900 ppm of H_2O.

Mixtures of 10, 30 and 50 wt% of as-fabricated UN microspheres (52 %TD) and $UO_{2.13}$ powder, as well as pure $UO_{2.13}$ and UN microspheres, were sintered by the spark plasma sintering (SPS) method at the National SPS Facility in Stockholm/Sweden. This method is a field-assisted sintering technology, which uses low voltage and high current combined with an applied pressure to consolidate powders [33,34]. The mixtures of $UO_{2.13}$ powder and as-fabricated UN microspheres (~4 g in total) were prepared inside a glovebox (< 0.1 ppm O_2) connected to the SPS machine. The mixtures were manually homogenised in a small beaker (25 mL) for 1 min with a spatula, poured out in an assembled graphite die (with graphite punches), and transferred to the SPS chamber (more details can be found in our previous article [28]). The SPS equipment used in this study is a modified Dr Sinter machine inside a glovebox, under argon atmosphere (< 0.1 ppm O_2), to minimise sample oxidation during preparation and sintering. The SPS chamber was depressurised to about 2 Pa to sinter the samples at 1773 K and 80 MPa, using the following thermal profile: heating at 100 K/min until 1573 K and then 50 K/min until 1773 K, held at this plateau for 3 min, and cooled to room temperature using two different cooling rates. First, a slow cooling (SC) profile: 10 K/min (1773-1573 K), 20 K/min (1573-1373 K) and 50 K/min (1373-973 K). Second, a fast cooling (FC) profile: 50 K/min (1773-1173 K). In both cases, from 973 K (SC) and 1173 K (FC) on, the cooling held naturally, i.e. no control over the cooling rate was applied. Additional details about the SPS equipment and sample preparation, as well as the sintering procedures, can be found in our previous article [28].

The samples are identified in this paper as UN(X)-UO_2 (SC/FC), where X is the initial weight fraction (wt%) of UN microspheres in the composite, and SC/FC specifies which cooling rate was applied. Table 1 reports the sample identifications and the SPS parameters used in this study.

2.2. Oxidation experiments

The oxidation kinetics of the samples were assessed by thermogravimetric analyses (TGA) in a synthetic air flow of 20 mL/min, using a TGA Discovery equipment (TA Instruments) with a weight

Table 1
Sample identification and the spark plasma sintering parameters.

Material	UN microsphere (wt%)	Cooling rate (K/min)	Sample identification
$UO_{2.13}$ powder	0	10 (1773-1573 K), 20 (1573-1373 K) and 50 (1373-973 K)	UO_2 (SC)
UN microsphere	100	10 (1773-1573 K), 20 (1573-1373 K) and 50 (1373-973 K)	UN (SC)
UN-UO_2	10	50 (1773-1173 K)	UN(10)-UO_2 (FC)
UN-UO_2	30	10 (1773-1573 K), 20 (1573-1373 K) and 50 (1373-973 K)	UN(30)-UO_2 (SC)
UN-UO_2	30	50 (1773-1173 K)	UN(30)-UO_2 (FC)
UN-UO_2	50	50 (1773-1173 K)	UN(50)-UO_2 (FC)

All samples were sintered at 1773 K and 80 MPa for 3 min. SC = slow cooling. FC = fast cooling.

sensitivity of 0.1 µg. The samples were placed in a platinum pan without cover and heated up to 973 K at 5 K/min, held at this plateau for 10 min, and then cooled to room temperature. Each sintered pellet (~3.5 g, ~6 mm x 5 mm diameter x height) was cracked in small pieces, and about 45 mg were used in the TG experiments. The weight variation (%) was defined as the percentage due to the weight gain during the oxidation reactions. Also, oxidation onset temperature (OOT) was defined as the temperature at which 5 % of the total weight variation was observed [20], while the maximum reaction temperatures (MRTs) were obtained by analyses of the first derivatives of the weight variation curves (%/min). These considerations are suitable to adopt a consistent basis of comparison between each sample.

Three TG replicate measurements were performed for each sample to assess the standard deviations of all mean values of total weight variation (%), OOTs, MRTs, as well as the repeatability and reliability of the TG results. The standard deviations of the mean values were calculated by dividing the standard deviation of each variable (i.e. total weight variation (%), OOTs, MRTs) by the square root of the number of repeated measurements made [35], which is equal to three in our study. As-fabricated $UO_{2.13}$ powder and uncrushed UN microspheres were also oxidised to provide insights about their oxidation behaviours and data for comparison with UO_2 (SC) and UN (SC) samples.

Additionally, differential scanning calorimetry (DSC) analysis was performed in a Netzsch STA 449 F3 Jupiter equipment under a synthetic air flow of 40 mL/min. Approximately 90 mg of UN(50)-UO_2 (FC) composite fuel was characterised by DSC to evaluate the thermodynamics involved during the oxidation of the three phases present in the sintered material, i.e. UO_2, UN and α-U_2N_3. The material was also heated at 5 K/min up to 973 K, kept at this temperature for 10 min, and cooled to room temperature.

2.3. Characterisation

UN microspheres and $UO_{2.13}$ powder were characterised by scanning electron microscopy (SEM) and X-ray diffraction (XRD) to evaluate their morphologies and crystalline structures, respectively. The SEM used in all analyses was an SEM FEI XL30 with the INCA software. The external surfaces of both compounds were examined using the secondary electrons (SE) detector. Bulk morphologies of sintered UN microspheres and $UO_{2.13}$ powder, UN (SC) and UO_2 (SC) samples, respectively, were examined after standard metallographic preparation (grinding and polishing) of pellets that were hot mounted in a phenolic resin with carbon filler. Colloidal silica suspension (OP-U, 0.04 µm, Struers) was used to perform a final polishing (2 min) to enhance the contrast between the grains of UO_2 (SC).

The XRD scans of the raw materials were carried out in a Siemens D5000 diffractometer with $Cu_{K\alpha}$ radiation (Ni filter), 2θ ranging between 20° and 120°, with 2θ step of 0.02° and acquisition time of 9 s for each step. The UN microspheres were milled inside a glovebox filled with argon (< 250 ppm O_2) using a mortar and pestle, and then encapsulated in an air-tight XRD specimen holder (Bruker model A100B138-B141) to avoid any oxidation during the analysis.

After sintering, the external surfaces of the samples were ground to remove the residual graphite foil from the SPS experiments. XRD and elemental analyses had been performed before in sintered pellets and the results showed that the C contents were consistent with the initial materials [36]. Therefore, grinding the sintered pellet surface is enough to remove the bounded graphite paper from SPS.

A modified Archimedean method, with chloroform as the immersion medium, was used to measure the sintered densities of all samples [36]. Afterwards, the sintered pellets were cut longitudinally and milled to powder using a mortar and pestle in an argon-filled glovebox (< 250 ppm O_2) for XRD analyses, using the same equipment, special holder, and parameters. The theoretical densities (TD) were computed based on the weight fractions of each phase after SPS using the Rietveld method and the software MAUD [37]. Before all XRD measurements, the software MAUD were configured with the information from the Siemens D5000 diffractometer (e.g. wavelengths, goniometer radius). Additionally, an instrumental broadening determination (with yttrium oxide) was performed before calculating the lattice parameters and the weight fractions after sintering [38]. The considered TD reference values [39] for UO_2, UN and α-U_2N_3 were 10.96 g/cm^3, 14.32 g/cm^3 and 11.24 g/cm^3, respectively. SEM examinations were performed in the polished longitudinal cross sections, coated with carbon, using both secondary and backscattered electron (BSE) detectors.

SEM-BSE images were used to estimate the average grain sizes of the UO_2 phase in the composites using the software ImageJ [40,41]. The averages were computed based on 5 measurements per grain, considering 20 grains per image and 3 images per sample. Brightness and contrast were adjusted to enhance the grain orientation contrasts. In total, 100 measurements per sample were collected and the average grain sizes, with 95 % confident intervals [35], were obtained from these values.

Post oxidised samples were examined using the same SEM equipment to analyse their surface morphologies. Energy-dispersive X-ray spectroscopy (EDS) was also used to identify the chemical elements present in the oxidised samples.

3. Results and discussion

3.1. Phase and morphology of the raw materials and non-oxidised samples

Fig. 1 (a) and Fig. 1 (b) report the morphologies of the $UO_{2.13}$ powder and UN microsphere, respectively. $UO_{2.13}$ powder's morphology was characteristic of the industrial ammonium uranium carbonate (AUC) wet route [42], with internal porosity that mainly contributes to the surface area of the material. UN microspheres were porous, with some cracks on the surface from the fabrication process, and had a density of about 52 %TD [28].

The XRD patterns of the $UO_{2.13}$ powder and UO_2 (SC) sample, as well as the UN microspheres and UN (SC) sample, are presented

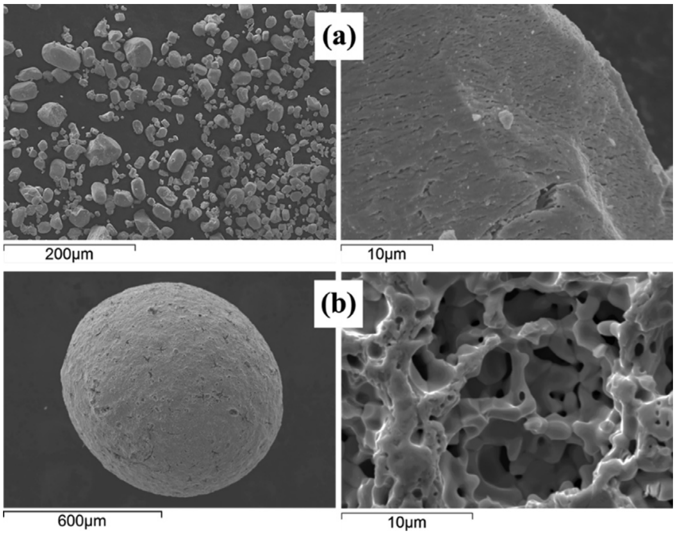

Fig. 1. SEM-SE images of the (a) $UO_{2.13}$ powder and (b) UN microsphere. $UO_{2.13}$ showed a characteristic ex-AUC powder morphology [42], with internal porosity that mainly contributes to the surface area of the material. The as-fabricated UN microspheres showed superficial and internal porosity with a density of ~52 %TD [28].

in Fig. 2 (a) and Fig. 2 (b), respectively. The computed lattice parameters were 0.5459 ± 0.0001 nm and 0.5475 ± 0.0001 nm (ref. 0.5470 ± 0.0001 nm [43]) for the $UO_{2.13}$ and UO_2 (SC) phases, respectively. The $UO_{2.13}$ data show broader peaks when compared to UO_2 (SC). This broadening can be attributed to peak overlap owing to the presence of secondary phases such as U_3O_7 and U_3O_8 [25]. Additionally, a lattice distortion as a result of excess oxygen in the UO_2 powder [43,44] can cause broadening. These higher oxide phases are intrinsically formed during the conversion process, where the $UO_{2.0}$ powder is pacified to UO_{2+x} [42,45]. Shifts in the position of the UO_2 peaks before and after sintering are observed in Fig. 2 (a). These shifts may be a result of the differences in the lattice parameters, as well as thermally induced residual stress in the UO_2 (SC) sample [46]. Previous studies [25,47] have also attributed the shifts to the variation in the lattice parameters caused by dissolved/excess of oxygen in the lattice, as well as to thermally induced residual stress.

The calculated lattice parameters for the UN microspheres and UN (SC) sample were 0.4887 ± 0.0004 nm and 0.4889 ± 0.0001 nm (ref. 0.4889 ± 0.0001 nm [48]), respectively. Both samples had cubic phases with equivalent lattice parameters, but showed very low intensity peaks at (about) 28° (111) and 33° (200), which correspond to the UO_2 phase originated from oxygen impurity.

Fig. 3 shows SEM images of the non-oxidised sintered samples. UO_2 (SC) micrographs in Fig. 3 (a) reports a dense microstructure with small and rounded pores (< 2 μm) on the grain corners, characteristic of closed porosity at the end of the sintering process [49]. In contrast, the UN (SC) sample in Fig. 3 (b) had a porous structure with large, irregular and interconnected open pores (< 14 μm). As studied by Johnson and Lopes [50], zero per cent of open porosity during SPS of UN fuel can be reached at 1650 K with holding pressures of 90-135 MPa and holding times of 2-15 min. In fact, the UN (SC) sample was still sintering at 1773 K after 3 min, as shown in our previous study [28]. This porosity in UN (SC), as a result of sintering coarse UN microspheres (when compared to UN powder [50]), was then originated from an incomplete pore rounding step during the last stage of sintering [49]. Both micrographs represent the sintered densities reported in Table 3: higher density for the oxide (97.5 %TD), and lower density for the nitride (83.8 %TD) pellets.

Table 2
Average grain sizes of the sintered samples computed using ImageJ [40,41], considering 5 measurements per grain, 20 grains per image, and 3 images per sample.

Sample Identification	Average grain size (μm)
UO_2 (SC)	3.2 ± 0.2; 5.6 ± 1.6[*]
UN (SC)	3.1 ± 0.4; 7.3 ± 0.2[†]
UN(10)-UO_2 (FC)	4.8 ± 0.4[♦]
UN(30)-UO_2 (SC)	8.1 ± 0.7[♦]
UN(30)-UO_2 (FC)	7.6 ± 0.6[♦]
UN(50)-UO_2 (FC)	9.5 ± 0.6[♦]

[*] Ge et al. (1623 K, 40 MPa, 5 min) [47].
[†] Johnson and Lopes (1723 K, 90 MPa, 3 min) [50].
[♦] Values related to the UO_2 matrix.

The UN-UO_2 composite fuel microstructures described in Fig. 4 (a-d) show that a third phase, α-U_2N_3 (sesquinitride), was formed during fabrication as a result of the interaction between UO_2 and UN [28]. Similar microstructural features were observed in a previous study of the reaction of UO_2 with carbon in the presence of N_2 at 1973 K [51]. Moreover, based on our previous article [28] and published data [12–14], the interaction between the UN and UO_2 does not depend on the sintering atmosphere and density/morphology/type of the UN phase. Yet, the interaction between the UN and UO_2 does not depend on the O/U ratio either. As demonstrated by [14], sintering $UO_{2.0}$ powder with dense UN pieces (125-1000 μm, 95.7-97.2 %TD) resulted in a second nitride phase. This behaviour may be due to the equilibium phase of UO_2, which describes that the oxide can be present as a hypo-stoichiometric phase (UO_{2-x}) at the sintering temperature and low oxygen potential [52]. The amount of each phase in the sintered materials affected the oxidation kinetics of the samples (details are described in the upcoming sections).

Our previous study [28] showed that sintering the UN-UO_2 composites at low temperatures (< 1173 K) and pressures (≤ 40 MPa), combined with a fast cooling profile, may minimise the amount of the α-U_2N_3 phase. Previous studies on the U-O, U-N, and quaternary system U-C-O-N [53–56] provide important information regarding the UO_2, U_2N_3, UN-U_2N_3, and UN-U_2N_3-UO_2 systems, as well as propose that the formation of the U_2N_3 phase during sintering may be minimised by either lowering the sintering temperature or changing the sintering atmosphere to argon.

Table 2 reports the average grain sizes of the UO_2 (SC) and UN (SC) samples, as well as of the UO_2 phase in the composites. The computed average grain size for UO_2 (SC) was 3.2 ± 0.2 μm, slightly different from a previous study (5.6 ± 1.6 μm) that used similar SPS parameters (1623 K, 40 MPa, 5 min) [47]. This difference may be due to an extra 2 min in the sintering time, since the authors found that the average grain size increases with the sintering time. UN (SC) sample's value was 3.1 ± 0.4 μm, lower than the result obtained by Johnson and Lopes [50]. The authors sintered UN powder by SPS at 1723 K (90 MPa, 3 min) and obtained an average grain size of 7.3 ± 0.2 μm. Since the expected sinterability of micro-sized powder is higher than coarse microspheres [49], this may be the reason why the authors found a larger average grain size. Regarding the composites, as a general rule, the higher the amount of nitride phases in the sample, the higher the average grain size of the UO_2 matrix. Since N forms a solid solution with the UO_2 matrix, such as $UO_{2-x}N_x$ [28], the grain growth was enhanced with the increase of the UN initial amount [49]. On the other hand, by only changing the cooling rate, the average grain size did not differ significantly when the uncertainties are considered.

Fig. 5 presents the powder XRD diffractograms of the sintered samples. In all composite fuels, a sesquinitride phase (α-U_2N_3) was

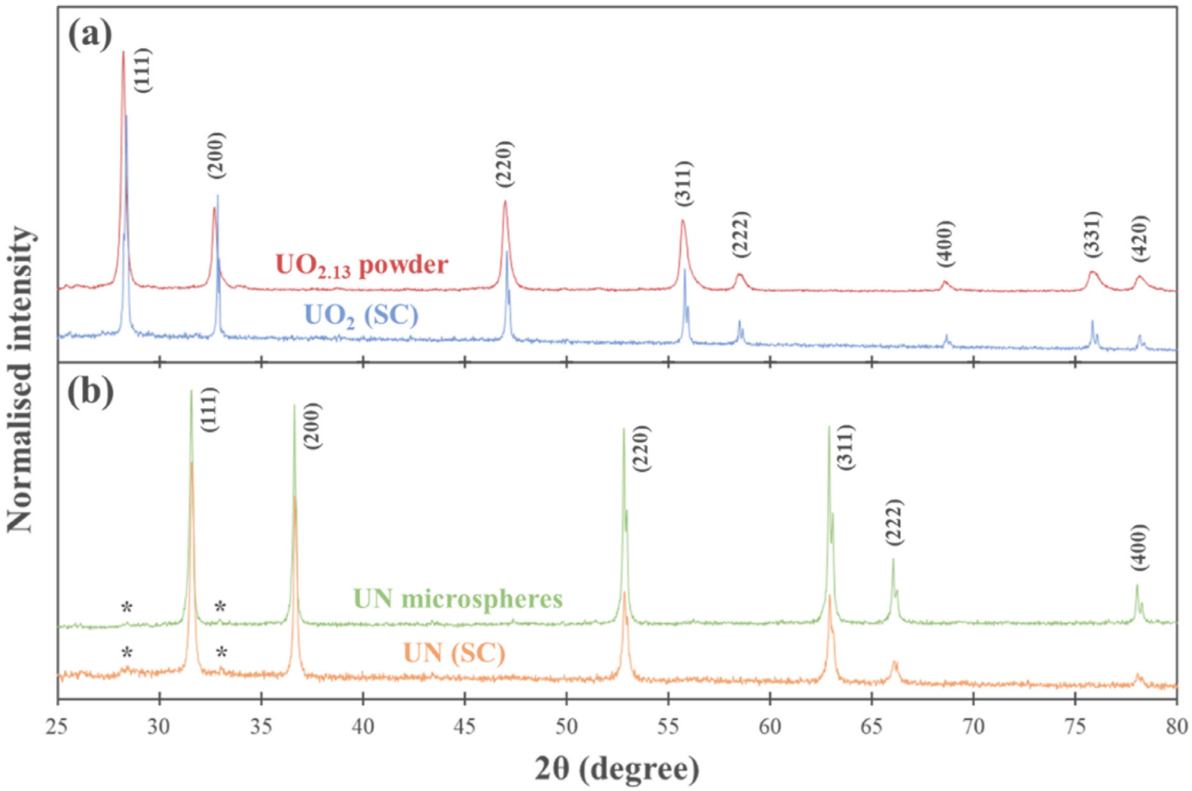

Fig. 2. X-ray diffraction patterns of the (a) $UO_{2.13}$ powder and UO_2 (SC) sample, and (b) UN microspheres and UN (SC) sample. $UO_{2.13}$ broadening peaks can be attributed to peak overlap owing to the presence of secondary phases such as U_3O_7 and U_3O_8 [25], as well as U_4O_9 [43,44]. Low intensity peaks (*) are present in the nitrides at (about) 28° (111) and 33° (200), which correspond to the UO_2 phase originated from oxygen impurity.

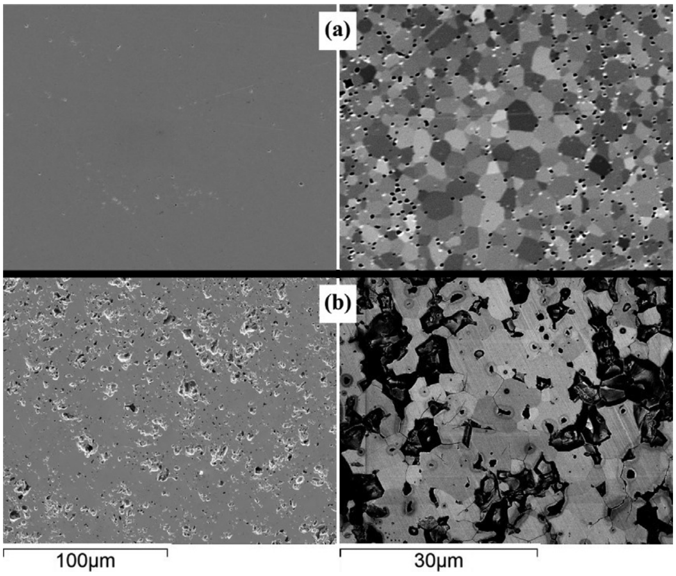

Fig. 3. Micrographs of non-oxidised (a) UO_2 (SC) and (b) UN (SC) samples. Higher magnification images better show the pores and grains morphologies. UO_2 (SC) had a dense microstructure with small and rounded pores (< 2 μm) on the grain corners, characteristic of closed porosity [49]. Conversely, UN (SC) had a porous structure with large, irregular and interconnected open pores (< 14 μm).

present, together with the UO_2 and UN initial phases. The amount of each phase, as well as the sintered and theoretical densities of all samples, are described in Table 3. The weight fractions of UN microspheres decreased in the composite fuels as a result of the interaction between the UN and UO_2 during fabrication, as demonstrated in our previous article [28]. The amounts of UN microspheres consumed/reacted during fabrication were then 87 %, 87 %, 63 % and 30 % for samples UN (10)-UO_2, UN (30)-UO_2 (SC), UN (30)-UO_2 (FC) and UN (50)-UO_2 (FC), respectively. Composite fuels with sintered densities of 91-96 %TD were obtained using SPS in just 3 min of sintering time.

From Table 3, the final α-U_2N_3/UO_2 wt% ratios for the samples UN(30)-UO_2 (SC), UN(30)-UO_2 (FC) and UN(50)-UO_2 (FC) were approximately 0.20, 0.21, and 0.21, respectively. Conversely, the ratio for the sample with (initially) 10 wt% of UN microspheres was ~0.04, which was the lowest value among the composites mainly due to the highest wt % of UO_2. Thus, for a higher initial amount of UN microspheres (30 wt%, 50 wt%), the final α-U_2N_3/UO_2 wt% ratios showed a similar trend in the final composites (~0.20). Furthermore, the sintered/original molar ratios of nitrogen for the UN(10)-UO_2 (SC), UN(30)-UO_2 (SC), UN(30)-UO_2 (FC) and UN(50)-UO_2 (FC) specimens were 0.66, 0.93, 1.13, and 1.03, respectively. These results indicate that most of the initial N was retained in the sintered composites, as experimentally observed during the sintering of pure UN microspheres and a UN-UO_2 composite; no significant variation in the vacuum pressure at high temperatures (> 773 K) [28].

3.2. Oxidation behaviour of the raw materials and ATF composites

TGA measurements were carried out in triplicate to assess the uncertainties and reliability related to the weight variations (%), OOTs and MRTs. However, for the sake of better visualisation, only one result per sample is presented in the following figures in the text. All measurements are available in Appendix A, which shows good repeatability and reliability of the experiments. Therefore, the results obtained from the microanalyses using TGA can be used as a starting point to understand the macro behaviour of the samples.

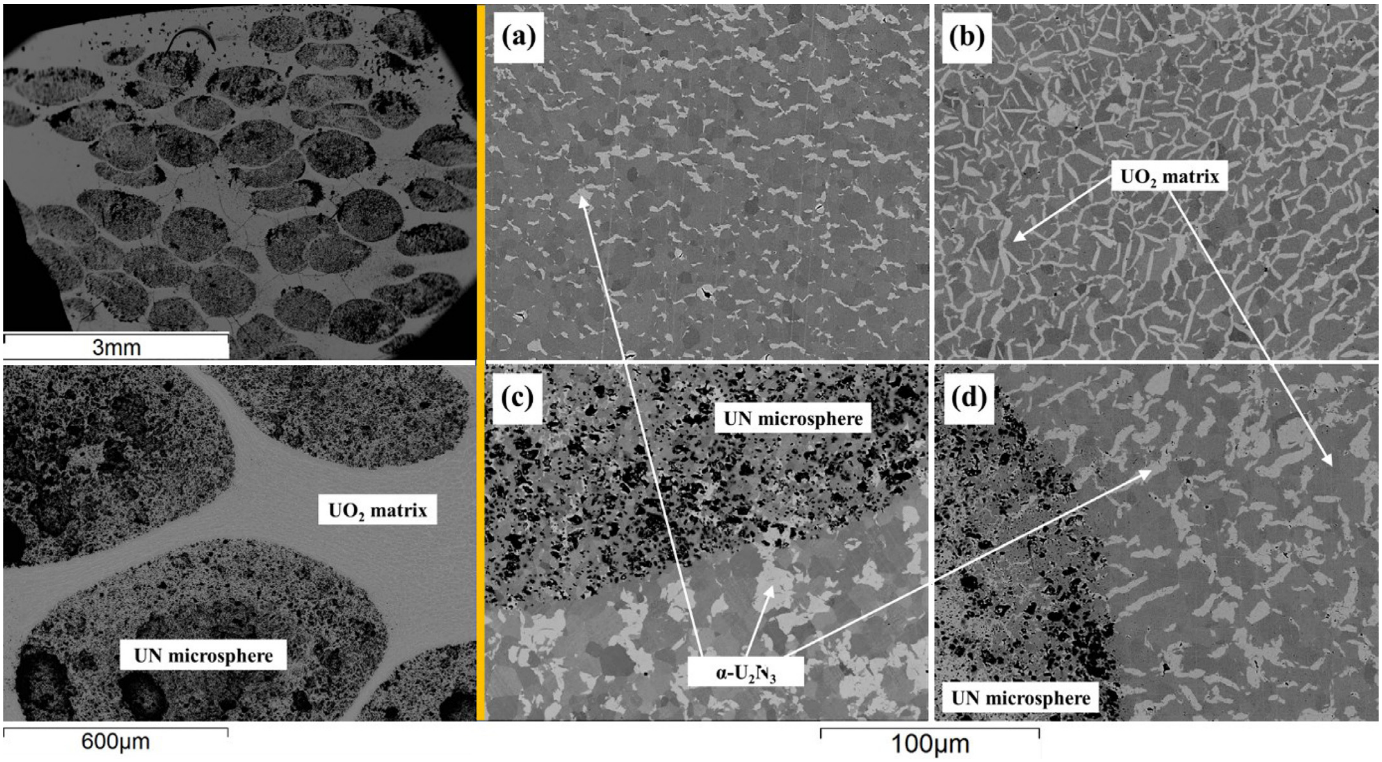

Fig. 4. SEM-BSE images of composite fuels showing (left) low magnification images, as well as samples (a) UN(10)-UO$_2$ (SC), (b) UN(30)-UO$_2$ (SC), (c) UN(30)-UO$_2$ (FC), and (d) UN(50)-UO$_2$ (FC). The composite microstructures were obtained from longitudinal cross-sections of the pellets at ~3 mm from the edge. The same microstructural features were observed near the pellet edges. A third phase indicated by the arrows, α-U$_2$N$_3$ (sesquinitride), was formed in all UN-UO$_2$ composite fuels. The amount of UN microspheres and the cooling rates affected the amount and/or shape of the sesquinitride phase (more details can be found in [28]).

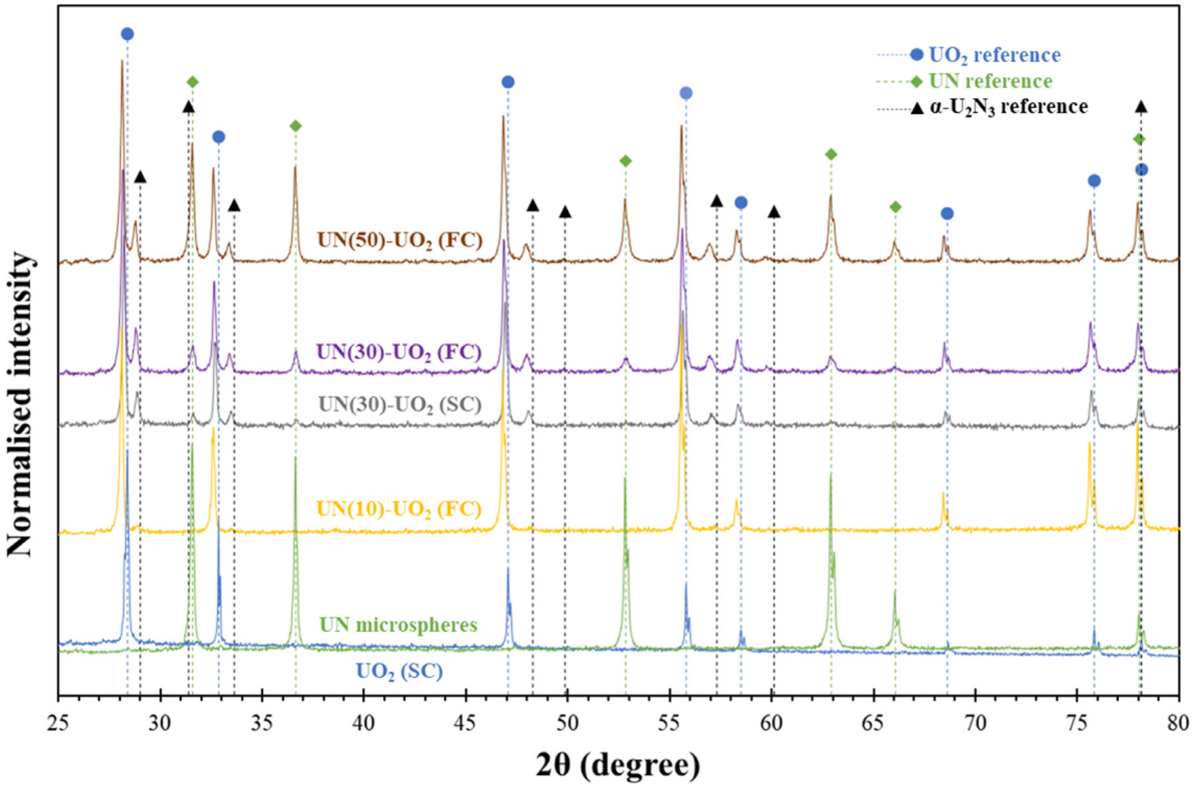

Fig. 5. X-ray diffraction patterns of the UO$_2$ (SC) and UN microspheres samples (references), as well as the UN-UO$_2$ composite fuels. Peaks related to the phase α-U$_2$N$_3$ (ICSD PDF 00-015-0426) are present in all sintered composites.

Table 3
Amount of phases and sample densities after sintering.

Sampleidentification	Amount of phases after sintering (wt%)*			Theoretical density (TD)† (g/cm^3)	Sintered density	
	UO_2	UN	α-U_2N_3		(g/cm^3)♦	(% TD)
UO_2 (SC)	100	0	0	10.96 [39]	10.69	97.5
UN (SC)	0	100	0	14.32 [39]	12.00	83.8
UN(10)-UO_2 (FC)	95.0 ± 0.8	1.3 ± 0.2	3.7 ± 0.3	11.02	10.47	95.1
UN(30)-UO_2 (SC)	79.8 ± 0.7	3.9 ± 0.2	16.3 ± 0.6	11.14	10.65	95.6
UN(30)-UO_2 (FC)	73.4 ± 0.5	11.1 ± 0.2	15.5 ± 0.4	11.38	10.78	94.8
UN(50)-UO_2 (FC)	53.8 ± 0.4	34.9 ± 0.3	11.3 ± 0.4	12.16	11.11	91.3

* Calculated from the XRD data using the Rietveld refinement method and the software MAUD [37].
† Computed based on the weight fractions and individual theoretical densities of UO_2 (10.96 g/cm^3), UN (14.32 g/cm^3), and U_2N_3 (11.24 g/cm^3) [39].
♦ Absolute densities measured by a modified Archimedean method, with chloroform as the immersion medium [36].

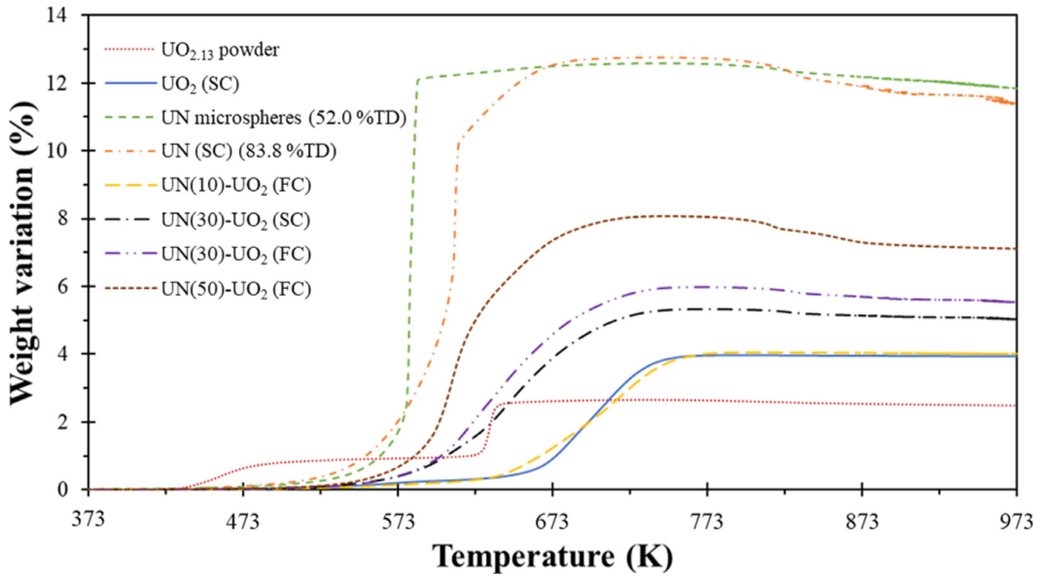

Fig. 6. Weight variations of all samples as a result of the oxidation reactions. Mass decreases at high temperatures (> 800 K) in the nitrides samples, as well as in the composites with 30 wt% and 50 wt% of UN microspheres, can be interpreted as nitrogen release from an intermediate oxynitride that is formed during the oxidation of the nitride phases [20,48].

Table 4
Theoretical oxidation reactions occurred in the oxidation thermogravimetric experiments, considering that the U_3O_8 phase was the ultimate product in all experiments [7,17,20,57].

Oxidation reaction	Equation	Remark
$3\ UO_2 + O_2 \rightarrow U_3O_8$	(1)	UO_2 (SC) pellet oxidation reaction.
$6\ UN + 8\ O_2 \rightarrow 2\ U_3O_8 + 3\ N_2$	(2)	UN (SC) pellet oxidation reaction.
$3\ U_2N_3 + 4\ O_2 \rightarrow 2\ U_3O_8 + 4.5\ N_2$	(3)	Oxidation of α-U_2N_3 present in the sintered samples.
$x\ UO_2 + y\ UN + z\ U_2N_3 + O_2 \rightarrow U_3O_8 + N_2$	(4)*	Overall oxidation reaction of the sintered samples.

* x, y and z are related to the amounts of UO_2, UN and α-U_2N_3, respectively, present in the sintered pellets (Table 3).

Weight variation (%) measurements of the specimens oxidised in a synthetic air atmosphere up to 973 K are shown in Fig. 6, which indicates the differences between the nitride, composites, and UO_2 behaviours. The mass decreases observed at high temperatures (> 800 K), in both the nitrides and composites with 30 wt% and 50 wt% of UN microspheres, are also observed in previous studies [24,48]. According to these previous studies, the mass decreases can be interpreted as the release of nitrogen (as N_2 gas) from an intermediate oxynitride product that is formed during the oxidation of the nitride phases. We have not detected nitrogen in the SEM-EDS examinations; only oxygen and uranium as chemical elements were present in all the oxidised samples.

Theoretical weight variations were obtained using the reactions described in Table 4, considering that the ultimate product in all experiments was U_3O_8 and that the nitrogen exits the samples as N_2 gas [7,17,20,57]. These theoretical values were compared to the ones obtained from the TG results, with their deviations described in Table 5 as a percentage change (% change). The errors associated to the real values were obtained by considering the maximum and minimum values from the TG results. The percentage change was defined as the difference between the theoretical and real values divided by the theoretical one. All samples showed small weight variation uncertainties (≤ ± 0.17%) and percentage changes (≤ 4.5 %), indicating that the equations in Table 4 can describe the oxidation of the specimens, as well as showing good repeatability of the experiments. The weight variation of UO_2 (SC) (3.94 %) was only 0.3 % different from the stoichiometric UO_2 pellet. When the errors in both real and theoretical values are considered, the weight gain (real) of the samples UN (SC), UN (30)-UO_2, and UN (50)-UO_2 can be considered equivalent to the respective theoretical values. Sample UN (10)-UO_2 was the only one that presented a real

Table 5
Average values of the weight variations, oxidation onset temperatures, and maximum reaction temperatures of the sintered samples.

Sample Identification	Weight variation (%)			Oxidation onset temperature (OOT) (K)†	Maximum reaction temperature (MRT) (K)♦
	Theoretical	Real	% Change*		
UO_2 (SC)	3.95	3.94 ± 0.00	0.3	570 ± 5	704 ± 2
UN (SC)	11.37	11.25 ± 0.15	1.1	533 ± 2	604 ± 9
UN(10)-UO_2 (FC)	4.21 ± 0.08	4.02 ± 0.01	4.5	593 ± 6	713 ± 3
UN(30)-UO_2 (SC)	4.96 ± 0.10	5.02 ± 0.02	1.2	556 ± 1	641 ± 4
UN(30)-UO_2 (FC)	5.46 ± 0.08	5.57 ± 0.05	2.1	560 ± 5	618 ± 3
UN(50)-UO_2 (FC)	7.04 ± 0.08	7.10 ± 0.17	0.9	557 ± 1	610 ± 2

* % Change = 100 x |Real – Theoretical| / Theoretical.

† Oxidation onset temperature (OOT) is defined as the temperature at which 5 % of the total weight variation was observed.

♦ Maximum reaction temperatures (MRTs) were obtained by analyses of the first derivatives of the weight variation curves.

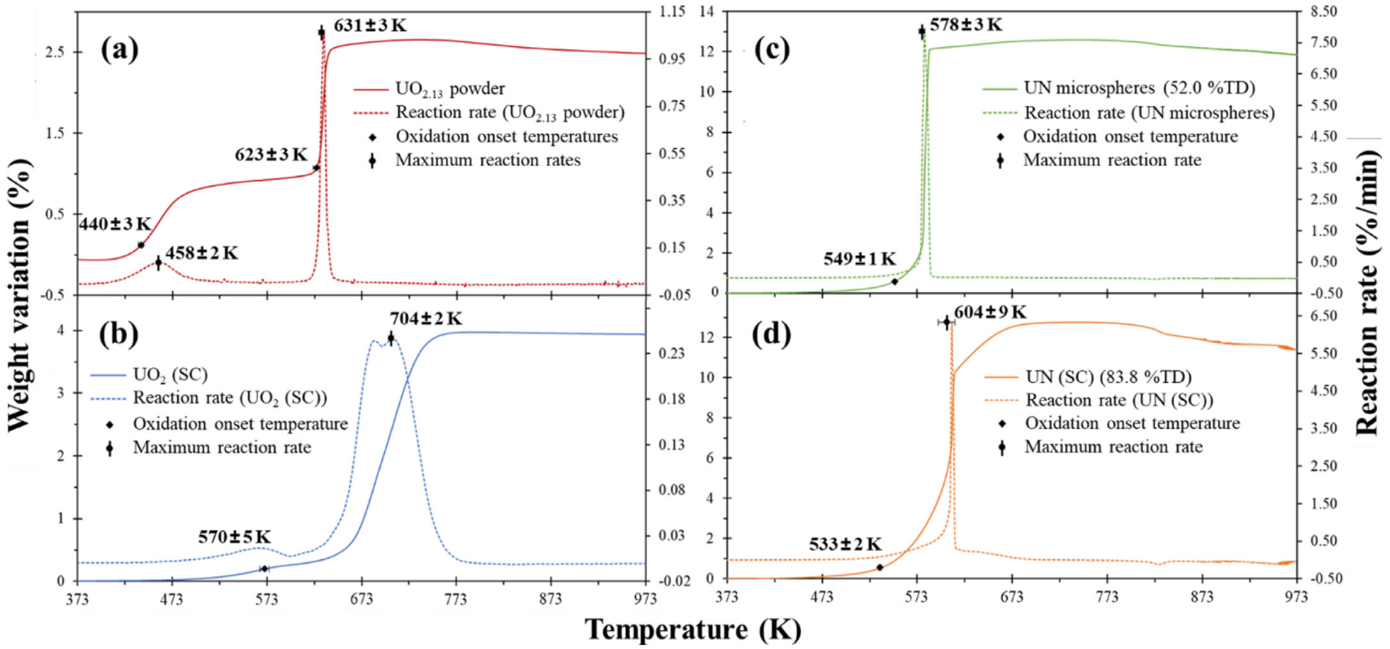

Fig. 7. Weight variation curves (solid lines) and reaction rates (dashed lines) of (a) $UO_{2.13}$ powder, (b) UO_2 (SC), (c) UN microspheres (52.0 %TD), and (d) UN (SC) (83.8 %TD). The average values and the uncertainties of the oxidation onset temperatures (OOTs) and the maximum reaction temperatures (MRTs) are indicated in the graphs. $UO_{2.13}$ powder showed a two steps oxidation curve, while the other samples had a single sigmoid shape: oxidation of UO_2 (or UN) into U_3O_8.

value slightly inferior to the theoretical one (the highest percentage change, 4.5 %).

The weight variation of the UO_2 (SC) sample (3.94 %) in Table 4, when compared to the theoretical value (3.95 %), indicates that the $UO_{2.13}$ powder reduced to stoichiometric UO_2 during sintering. Previous studies using spark plasma sintering [47] and conventional sintering [58–60] in vacuum atmospheres demonstrated that the UO_{2+x} powder was reduced to $UO_{2.0}$ during the sintering process. Ge et al. [47] justified the powder reduction as a result of the interaction between the graphite foil (from the SPS die) and UO_{2+x} to form UC on the pellet surface (XRD result). After grinding the pellet to remove the graphite foil, only the UO_2 phase was present in the XRD diffractogram. Kutty et al. [58] studied the sintering behaviour (dilatometry) of $UO_{2.15}$ up to 1673 K in vacuum, demonstrating that the shrinkage curves for vacuum exactly coincided with that for Ar and Ar-8 % H_2. Therefore, the reduction of UO_{2+x} to $UO_{2.0}$ can happen independent of the sintering process (SPS or conventional sintering) and sintering atmosphere (Ar, vacuum, H_2).

The oxidation onset and maximum reaction temperatures, extracted from the weight variation curves (Fig. 7, Fig. 8, Fig. 9), are summarised in Table 5. The uncertainties related to both OOTs and MRTs are also described, showing a minimum variation of ± 1 K and a maximum of ± 9 K.

Fig. 7 portrays the weight variation curves for the raw materials, UO_2 (SC) and UN (SC) samples. The first derivatives of each curve, here named as reaction rates, are also plotted in the figure. The oxidation of the $UO_{2.13}$ powder (Fig. 7 (a)) showed two oxidation steps: the first one is associated to a parabolic oxidation curve, while the second one is related to a sigmoid weigh variation curve. The first step corresponded to the formation of U_4O_9/U_3O_7 on UO_2 powders, following a diffusion-controlled mechanism [61]. The results showed an OOT and MRT of 440 ± 3 K and 458 ± 2 K, respectively, and a weight gain of 0.86 % up to 523 K, which is in agreement with the formation of the U_3O_7/U_4O_9 phases [57]. The second step, associated with a sigmoid curve, is interpreted as the oxidation of the U_3O_7/U_4O_9 phases into U_3O_8 by a nucleation and growth mechanism [62]. OOT and MRT of this step were 623 ± 3 K and 631 ± 3 K, respectively, with a total weight variation of 2.47 ± 1 %, which is in agreement with a previous TG analysis [63].

Fig. 7 (b) shows the complete oxidation of UO_2 (SC) into U_3O_8, with a total weight variation of 3.94 ± 0.00 %; quite similar to the nominal value of 3.95 % (Table 5). In the UO_2 (SC) case, the oxidation followed a sigmoid curve in one major step: from UO_2

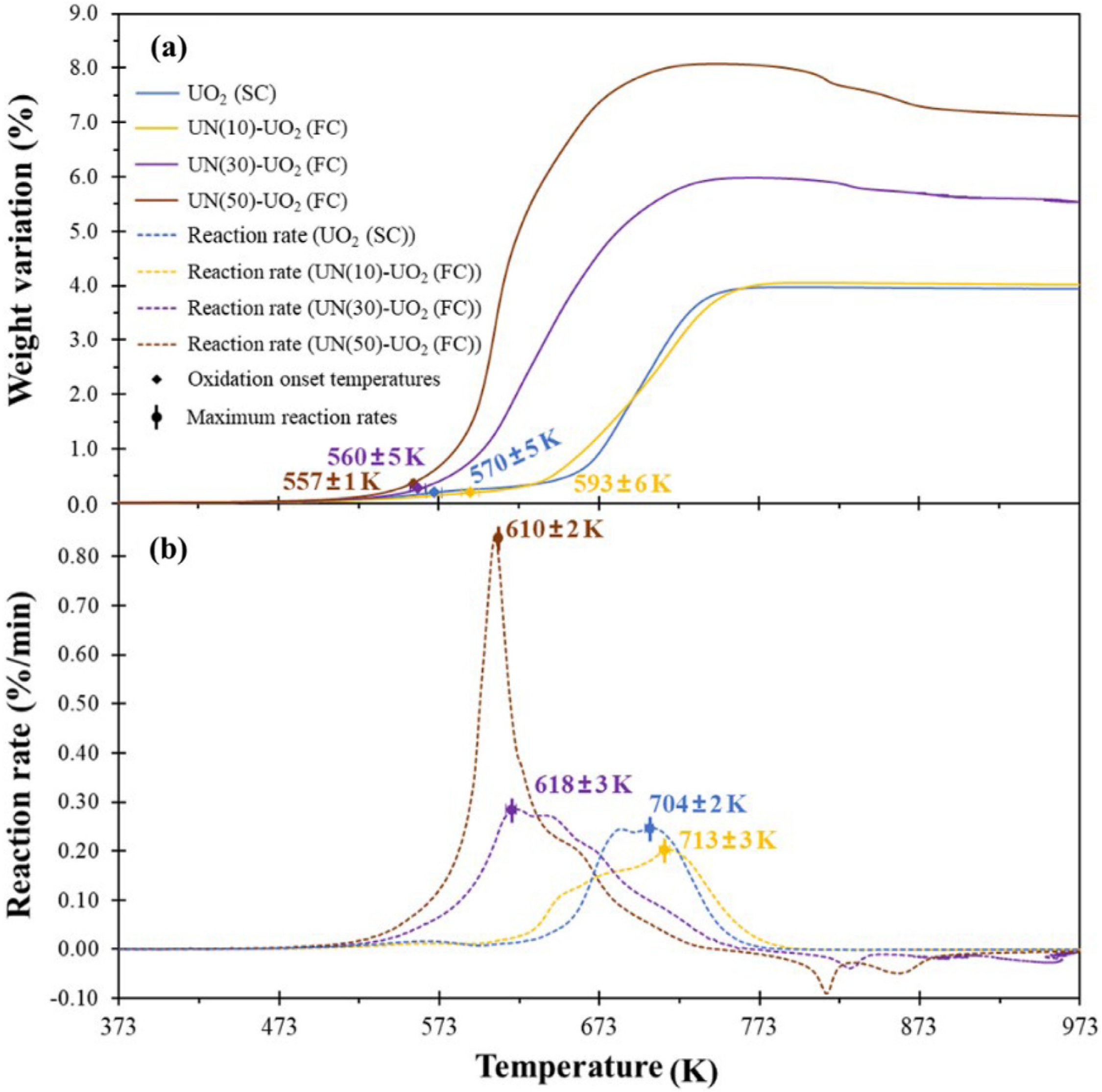

Fig. 8. Influence of the initial amount of UN microspheres (wt%) on the (a) weight variations and (b) reaction rates. The oxidation behaviour of UN(10)-UO_2 (SC) was similar to the UO_2 (SC) reference. The composite showed a higher OOT and MRT, as well as slower reaction rate at the maximum point. No changes in OOT was observed when the initial amount of UN microspheres changed from 30 wt% to 50 wt%. These results seemed to demonstrate that the UO_2 matrix provided a barrier against oxidation of the nitride phases.

to U_3O_8. The oxidation started with incubation time, at which a fine layer of U_3O_7 was formed on the external surface, followed by a parabolic kinetic (~623 – 680 K), and then a linear kinetic (~680 – 750 K) until the complete oxidation into U_3O_8 [57,61]. The OOT (570 ± 5 K) and MRT (704 ± 2 K) for UO_2 (SC) were higher than the $UO_{2.13}$ powder, since the oxygen chemisorption and the diffusion-controlled formation of U_3O_8 are both proportional to the surface area [57,64,65]. Thus, the higher the surface area, or the smaller the particle size, the faster the oxidation process.

UN microspheres and UN (SC) weight variation curves are presented in Fig. 7 (c) and Fig. 7 (d), respectively. The oxidation behaviours of both samples are similar, with sigmoid curves and total weight variation close to the nominal value of 11.37 %. The OOT for the UN microspheres (549 ± 1 K) was slightly higher than the UN (SC) (533 ± 2 K). As previously demonstrated [20], the oxidation resistance of the UN samples can be improved by eliminating open porosity. In our case, however, open porosity was not the only parameter that affected the oxidations. Yet, since the densities of the UN samples were different, the surface areas of both samples were also different and impacted the oxidation behaviour. Thus, a combination of higher open porosity and surface area of the UN microspheres (52 %TD), compared to UN (SC) (83.8 %TD), resulted in an OOT increment of about 16 K. Regarding the MRTs, the microspheres showed a lower temperature and higher rate, indicating that the formation of U_3O_8 was faster after the formation of an oxide layer during the incubation time. These results were expected since the UN microspheres were porous, which provides more surface area to be attacked during oxidation. Our ongoing work is focused on optimising the UN-UO_2 composite by using denser (80-95 wt%, based on previous studies [66–68]) and coated UN microspheres to avoid the interaction between UN and UO_2, as well as to delay the oxidation onset temperature of the UN microspheres.

The amount of UN microspheres affected the oxidation kinetics of the composite fuels, as reported in Fig. 8. For the same cooling rate, e.g. fast cooling (FC), the higher the UN content in the sintered composites, the higher the total weight variation. Additionally, there was a sesquinitride phase in the sintered composites, α-U_2N_3, that formed during fabrication as a result of the interaction between UN and UO_2 (Fig. 4, Fig. 5, [28]). The oxidation of this sesquinitride also contributes to increasing the total weight varia-

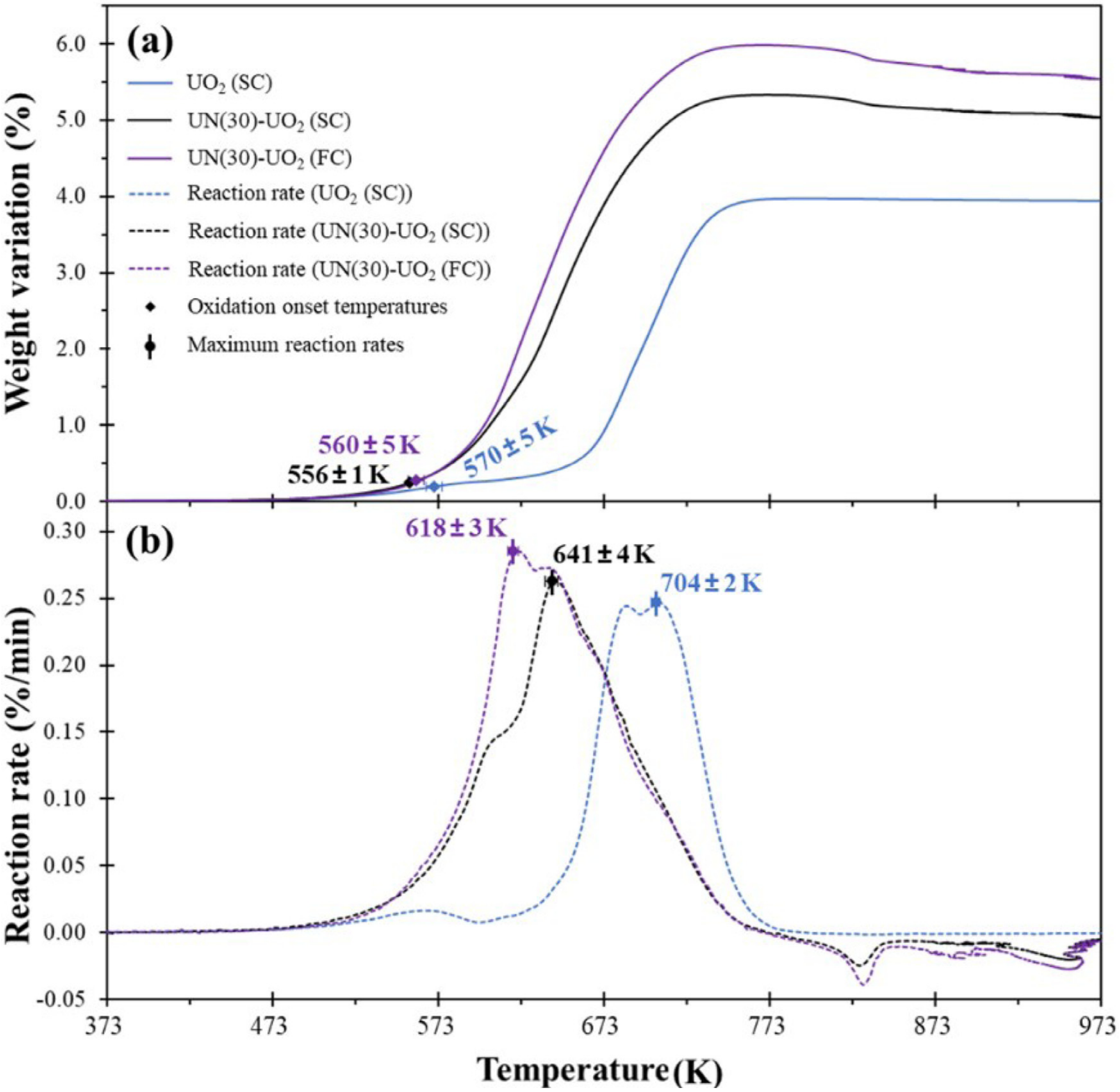

Fig. 9. Influence of the cooling rate on the (a) weight variations and (b) reaction rates. OOTs for the composites were similar to the UO_2 (SC) reference, indicating that the UO_2 matrix acted as a barrier to retard the oxidation of the nitride phases. The faster the cooling, the lower the MRT. This behaviour is directly affected by the highest amount of UN + α-U_2N_3 in the sample UN(30)-UO_2 (FC): 26.7 wt% against 20.2 wt% (slow cooling).

tions. As reported in Table 3, the total amount of UN + α-U_2N_3 in UN(10)-UO_2 (FC), UN(30)-UO_2 (FC) and UN(50)-UO_2 (FC) were 5.0 wt%, 26.6 wt% and 46.2 wt%, respectively. Regarding the grain sizes of the UO_2 phase of the composites (Table 2), the higher the initial weight fraction of UN microspheres, the larger the average oxide grain sizes in the final pellets. The initial oxidation rates, up to (about) 50 % yield, were faster when the matrix grain sizes increased. Quémard et al. [69] found that the oxidation rate up to ~ 50 % yield increased when the grain sizes diminished. This different behaviour might be because they were analysing pure UO_2 sample, as well as owing to additional complexity of the UN-UO_2 system: sesquinitride precipitates along and inside the UO_2 grain and UN embedded microspheres. Therefore, the initial oxidation rates in Fig. 8 depended not only on the average oxide grain sizes, but also on the nitride amounts in the sintered samples, which seemed to impact much more the rates than the grain sizes themselves.

Fig. 8 also reports the influence of the initial amount of microspheres on the OOTs and MRTs. The OOT of UN(10)-UO_2 (SC) (593 ± 6K) was surprisingly 23 K higher than the reference UO_2 (SC). Additionally, the composite showed a slightly higher MRT and lower oxidation rate at the maximum point, indicating that the oxidation reaction was more moderate in the composite than in the UO_2 (SC) reference. A previous study [23] proposed that the formation of U-N-O compounds on the surface of nitrided uranium can resist the diffusion of oxygen ions into the inner layer. Also, Lu et al. [19] showed that the corrosion resistance of the U_2N_3 phase is better than the U or UN phase structure films. Thus, the complexity related to the U-O-N system seems to retard the oxygen diffusion through the sample in some cases. Increasing the initial amount of UN microspheres from 10 wt% to 30 wt% and 50 wt% have not affected the OOTs. Also, these composites had similar OOTs when compared with the UO_2 (SC) reference. These results seemed to demonstrate that the UO_2 matrix provided a barrier against oxidation of the nitride phases. However, the reaction occurred approximately three times faster in UN(50)-UO_2 (FC) (0.84 ± 0.14 %/min) than in UN(30)-UO_2 (FC) (0.29 ± 0.01 %/min) at the maximum rates, since the amount of nitrides was the highest in UN(50)-UO_2 (FC).

The influence of the cooling rates on the oxidation kinetics is reported in Fig. 9. The faster the cooling, the higher the nitride amounts in the sintered composite and, consequently, the greater

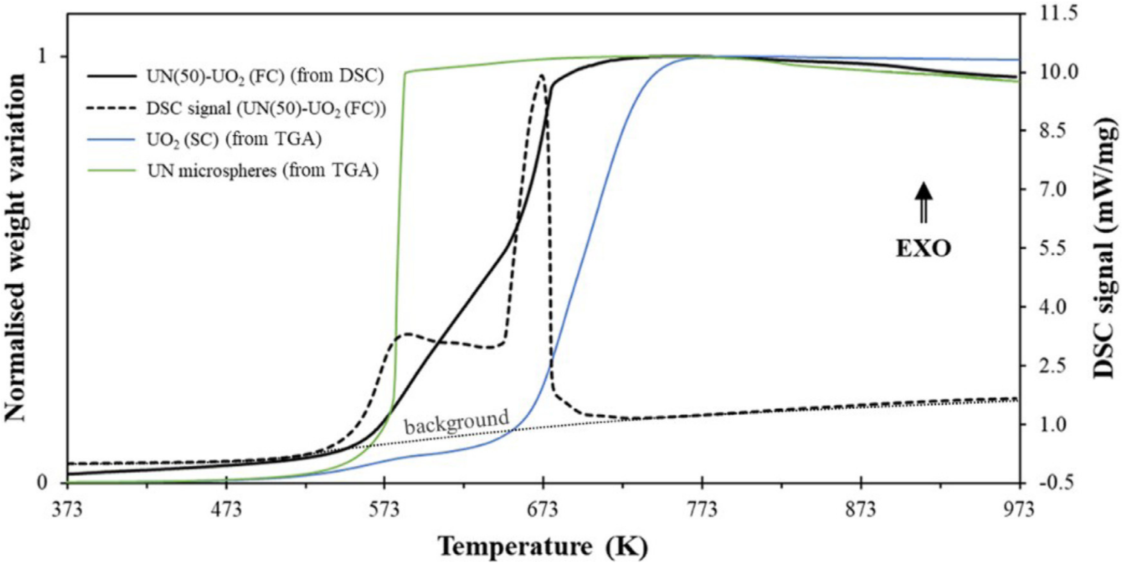

Fig. 10. Differential scanning calorimetry analysis of UN(50)-UO_2 composite fuel heated at 5 K/min up to 973 K at 40 mL air/min. Normalised UO_2 (SC) and UN microspheres weight variations (from TGA) are plotted as illustrative references. The DSC data showed two linear kinetic regions associated with exothermic peaks: 573-650 K and 660-685 K. Additionally, the UO_2 addition reduced the severity of the oxidation reaction and retarded the oxidation of the nitride phases.

the total weight variation. Samples UN(30)-UO_2 (SC) and UN(30)-UO_2 (FC) had a total amount of nitrides of 20.2 wt% and 26.6 wt%, respectively (Table 3). Concerning the OOTs reported in Fig. 9 (a), the cooling rate affected neither the chemisorption of oxygen onto the composites, nor the diffusion-controlled formation of U_3O_8 during the early oxidation stage ($<$ 523 K) [57,64,65]. Thus, the OOTs for the composites were quite similar to the UO_2 (SC) reference, when the uncertainties are considered, demonstrating that the UO_2 matrix retard the oxidation of the nitride phases. Nevertheless, the MRTs were affected by the cooling rate (Fig. 9 (b)). In the case of UN(30)-UO_2 (FC), the oxidation reaction reached a maximum of 0.29 ± 0.01 %/min at 618 ± 3 K, while the slowly cooled sample showed a slightly lower reaction rate (0.26 ± 0.01 %/min) at a higher temperature (641 ± 4 K). Therefore, the cooling rate affected directly the amount of UN + α-U_2N_3 in the composites and, consequently, the oxidation kinetics: the faster the cooling, the higher the amount of nitrides and the reaction rate, and the lower the MRT.

From the DSC data plotted in Fig. 10, two linear kinetic regions associated with exothermic peaks are observed: first, between 573 K and 650 K; and second, between 660 K and 685 K. At these regions, a proposed mechanism for the composite oxidation is that the reaction occurred via UO_2 grain boundary attack at fresh UO_2 surfaces that formed during cracking and nucleation/growth of U_3O_8 after an incubation time [57,65,69,70]. Simultaneously to the grain boundary attack, the α-U_2N_3 phase oxidised since it was present along and inside the UO_2 grains (Fig. 4). With the extent of reaction, the embedded UN microspheres were also reached by oxygen and resulted in a strong exothermic DSC peak at 673 K, which is characteristic of a highly exothermic nitride phase oxidation [15]. Therefore, the UO_2 addition was beneficial to retard and smooth the oxidation of the nitride phases.

3.3. Post oxidation morphology

Fig. 11 shows the micrographs of the as-fabricated and oxidised $UO_{2.13}$ powder, UO_2 (SC), UN microspheres, and UN (SC) samples. $UO_{2.13}$ powder's overall morphology has not changed after its oxidation, which is known to have a complex kinetic above 473 K owing to a simultaneous formation of U_3O_7 and U_3O_8 [71]. Since the powder had an initial surface area of 5.33 m^2/g, with most of it coming from internal porosity(Fig. 1 (a)), a net increase of ~36 % in volume due to its oxidation to U_3O_8 [70] might have been compensated by porosity and, then, avoided macro-cracking. Conversely, the oxidised UO_2 (SC) sample showed a general surface roughening and spalling after oxidation, as illustrated by SEM-SE images of a fragment in Fig. 11. As previously presented in [57,61] and discussed in section 3.2, the U_3O_8 formation on the UO_2 (SC) pellet occurred after the formation of a U_3O_7 layer at the beginning of the reaction. This layer increased until reaching a critical thickness and then spalled from the UO_2 as powder, generating cracks at the pellet surface. These cracks can be associated with a stress state created by the U_3O_7 on UO_2, since the U_3O_7 phase has a smaller lattice parameter than the UO_2 phase [69]. Afterwards, the oxidation reaction continued via grain boundary attack, with simultaneous cracking and nucleation/growth of U_3O_8 at the freshly created surfaces via linear kinetics until consuming all UO_2 [57,65,69,70]. Fig. 11 shows that macro-cracks were mostly formed at the UO_2 grain boundaries, with some micro-cracks inside the grains as well. Additionally, there are small fragments in the image that could have been generated during transportation, since the cohesive forces in the oxidised UO_2 samples are weak and may crack into powder when weak stress is applied [69].

UN microspheres and UN (SC) samples showed similar oxidation kinetics (Fig. 7 (c,d)) and post oxidised microstructures (Fig. 11). As a general behaviour, the growth mechanism of the U_3O_8 phase might have followed a succession of steps, such as adsorption of oxygen on the external surface, including inside the microspheres' open pores, and external interface reaction followed by diffusion through the U_3O_8 towards the freshly UN internal phase. The cracks observed in the UN samples seemed to occur at the beginning of the sigmoid curves, after reaching a critical oxide layer (similar to the UO_2 pellet) [57,61], and then inducing a rapid increase of the oxidation rates (Fig. 7 (c,d)) due to new reactive and fresh surfaces of UN. Furthermore, oxidation along grain boundaries introduced large stresses that the brittle nitride samples were unable to withstand. Similar intergranular cracking and spalling behaviours have been observed during hydrothermal oxidation of UN at 523-623 K and pressures up to 16.5 MPa [25], as well as during steam oxidation at 573 K and 9 MPa [21].

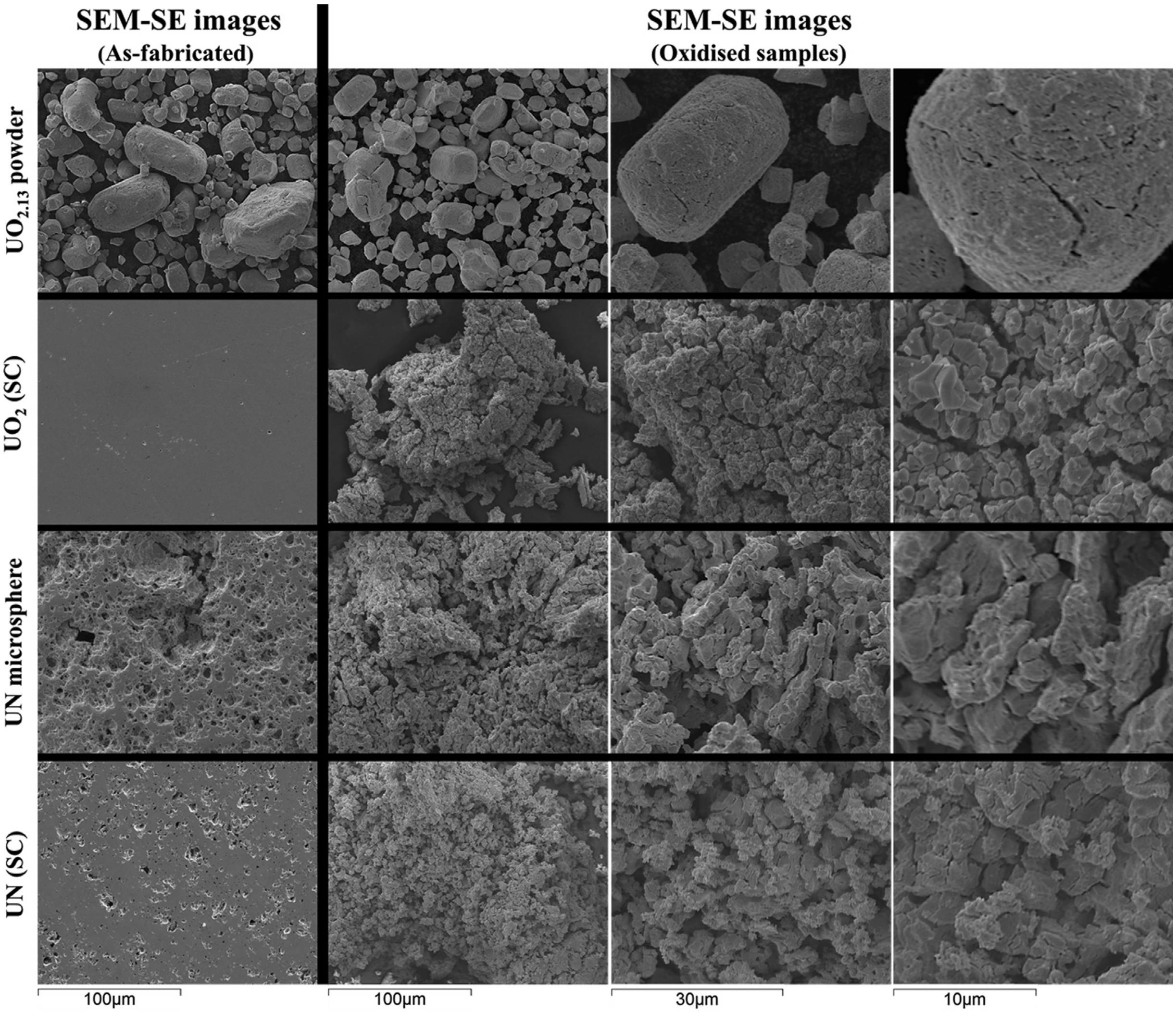

Fig. 11. Micrographs of as-fabricated and oxidised $UO_{2.13}$ powder, UO_2 (SC), UN microspheres, and UN (SC) samples. $UO_{2.13}$ powder's morphology did not change significantly after oxidation. Similar post oxidised microstructures with mostly intergranular cracking and spalling were observed in the UO_2 (SC) and nitrides samples.

Fig. 12 reports the micrographs of the as-fabricated and oxidised UN-UO_2 composite fuels. In general, the oxidised morphologies showed a corroded surface with intergranular cracking and spalling, and some intragranular cracks as well. As discussed in section 3.2, the formation of a critical oxide layer generated cracks at the surfaces, which enhanced the reaction rates by nucleation and growth of U_3O_8 on a freshly surface. Ex-situ SEM examinations did not allow a complete visualisation on how the oxidation reactions evolved. A previous article reports in-situ oxidation of UO_2 fuel pellet at 603 K and P_{O2} = 265 Pa up to 5.5 h [69]. The authors demonstrated that two types of cracks occurred during oxidation: first, macro-cracks occurred at the grain boundaries after 30 min of isothermal oxidation, followed by micro-cracking at the cracked surfaces that enhanced spallation. They also showed that the sample was still oxidising when the pellet was completely cracked with a constant weight variation, i.e. no more reactive surfaces was created. At this final stage, nucleation and growth of U_3O_8 proceeded until the total consumption of the UO_2 phase.

4. Conclusions

This article is presenting, for the first time, thermogravimetric experiments in triplicates concerning the oxidation resistance of high-density (91-97 %TD) UN/U_2N_3-UO_2 composite fuels in a synthetic air atmosphere bellow 973 K. The results show that the oxidation resistance of the composite with initially 10 wt% of UN microspheres is surprisingly better than the UO_2 reference. The OOT of UN(10)-UO_2 (SC) (593 ± 6 K) is about 23 K higher than the reference UO_2 (SC). Additionally, this composite shows a slightly higher MRT and lower reaction rate at the maximum rate, indicating that the oxidation reaction is smoother in the composite than in the UO_2 (SC). Additionally, there is no significant difference in the OOTs (~560 K) and MRTs (~613 K) when using 30 wt% or 50 wt% of embedded UN microspheres. These behaviours are a direct result of the improved oxidation resistance provided by the UO_2 phase, which acts as a protective barrier for the nitride phases. Nevertheless, the oxidation reaction occurs approximately three times faster in UN(50)-UO_2 (FC) (0.84 ± 0.14 %/min) than in UN(30)-UO_2 (FC) (0.29 ± 0.01 %/min) at the maximum rates, since the total amount of nitrides (UN + α-U_2N_3) is the highest in UN(50)-UO_2 (FC) (46.2 wt%). Regarding the cooling rates, the faster the cooling process during fabrication, the higher the total nitride contents in the sintered composites. This behaviour results in an expected higher total weight variation in UN(30)-UO_2 (FC) (5.57 ± 5 %) than in UN(30)-UO_2 (SC) (5.02 ± 2 %).

DSC analysis of UN(50)-UO_2 (FC) demonstrates more clearly that the oxidation of the composite fuels seems to follow two linear kinetics regions at 573-650 K and 660-685 K. At these regions,

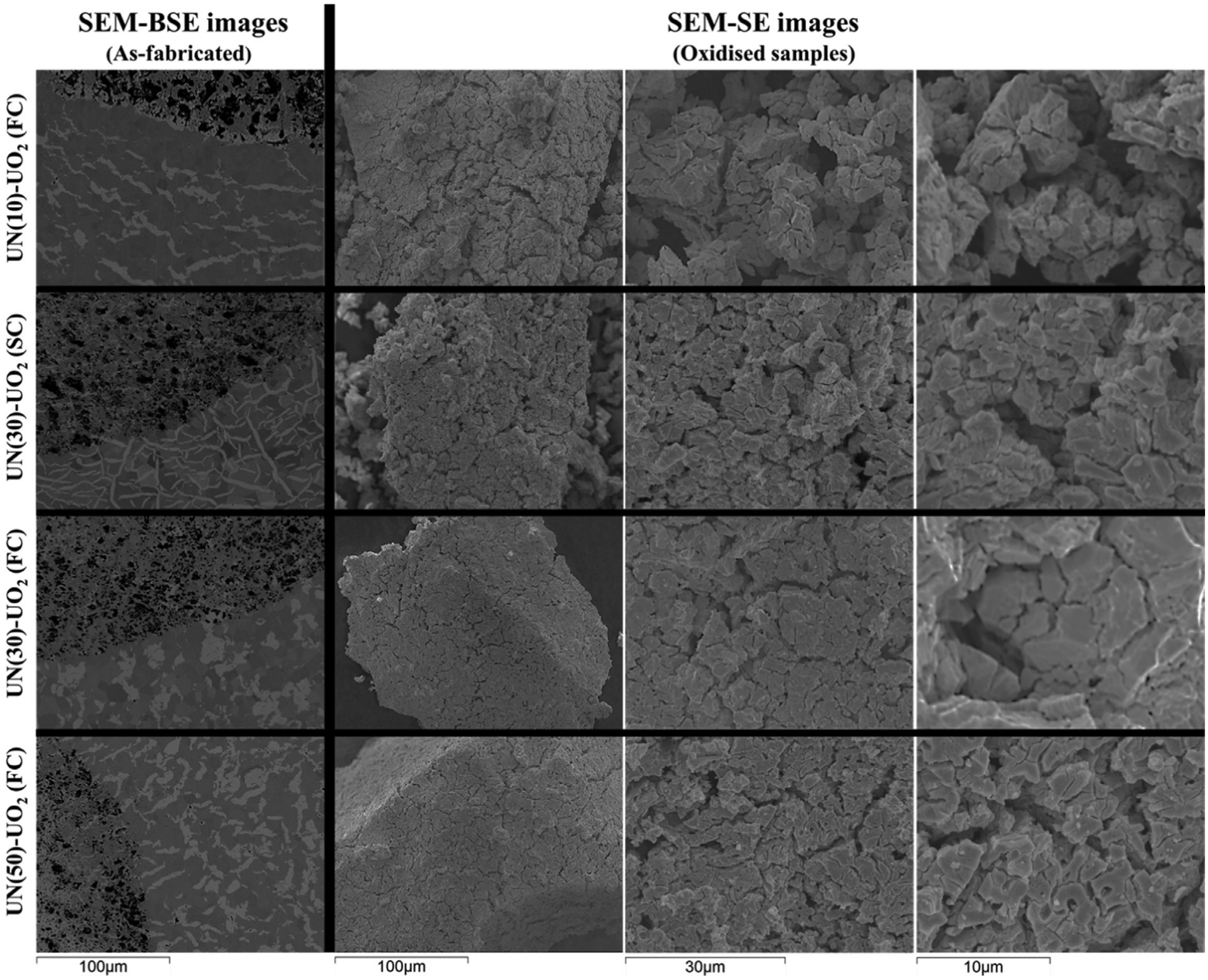

Fig. 12. Micrographs of as-fabricated and oxidised UN(10)-UO_2 (FC), UN(30)-UO_2 (SC), UN(30)-UO_2 (FC), and UN(50)-UO_2 (FC) composite fuels. All the oxidised morphologies had a corroded surface with mostly intergranular cracking and spalling, with some intragranular cracking as well.

a proposed mechanism is that the oxidation occurs via UO_2 grain boundary attack at freshly exposed UO_2 surfaces that are formed during cracking and nucleation/growth of the U_3O_8 phase. During the grain boundary attacks, it is suggested that the α-U_2N_3 phase oxidise since it is present along and inside the UO_2 grains. With the extent of reaction, the UN phase is also reached by oxygen and results in a strong exothermic DSC peak at 673 K. The oxidised composites have similar morphologies, showing a corroded surface with mostly intergranular cracking and spalling as a result of the oxidation reactions. Furthermore, the nitrides and UO_2 (SC) microstructures have a general roughening and spalling with intragranular and some intergranular cracks. Conversely, the overall morphology of the $UO_{2.13}$ powder does not change after its oxidation.

The findings in this study demonstrate that the UO_2 matrix acts as a barrier to improve the oxidation resistance of the nitride phases as they would exist at the beginning of life conditions. Therefore, the use of the UO_2 fuel to protect the UN microspheres is promising and requires future developments/tests to be used as an accident tolerant fuel in LWR.

Declaration of Competing Interest

The authors declare that they have no known competing financial interests or personal relationships that could have appeared to influence the work reported in this paper.

CRediT authorship contribution statement

Diogo Ribeiro Costa: Conceptualization, Methodology, Validation, Formal analysis, Investigation, Writing - original draft, Visualization. **Marcus Hedberg:** Investigation, Writing - review & editing. **Simon C. Middleburgh:** Writing - review & editing, Funding acquisition. **Janne Wallenius:** Funding acquisition. **Pär Olsson:** Resources, Supervision, Project administration, Funding acquisition. **Denise Adorno Lopes:** Conceptualization, Validation, Writing - review & editing, Supervision.

Acknowledgments

Financial support from Swedish Foundation for Strategic Research (SSF, *Stiftelsen för Strategisk Forskning*) is acknowledged [Project reference number ID17-0078]. SCM is supported through the Sêr Cymru II programme funded through the Welsh European Funding Office (WEFO) under the European Regional Development Fund (ERDF).

Appendix

All TGA experiments were performed in triplicate. The results for the raw materials, as well as for the UO_2 (SC) and UN (SC) samples, are plotted in Fig. A1. The coloured/bolded graphs are the data used in the article, and the grey curves indicate the replicates. Fig. A2.

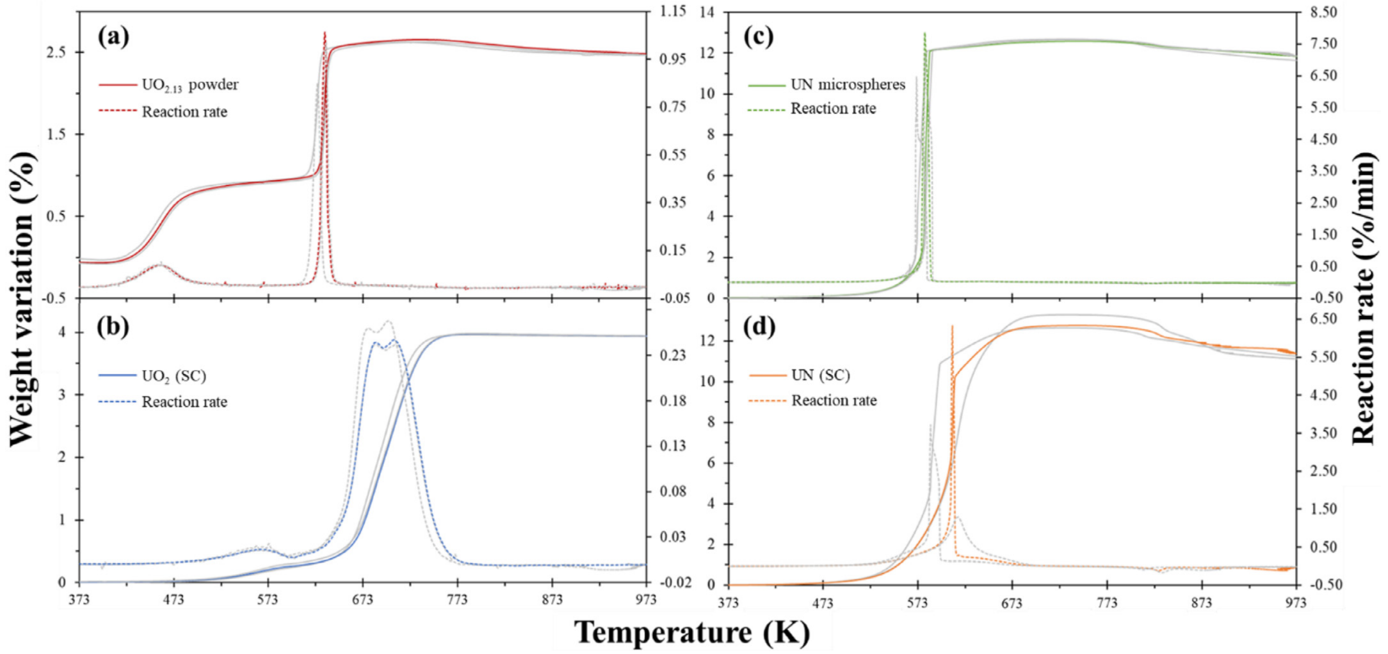

Fig. A1. Triplicate measurements of (a) $UO_{2.13}$ powder, (b) UO_2 (SC), (c) UN microspheres, and (d) UN (SC). The coloured/bolded curves are the ones used in the article. The results show good repeatability and reliability of the TGA experiments, with the largest discrepancy occurring in UN (SC) between 550-650 K.

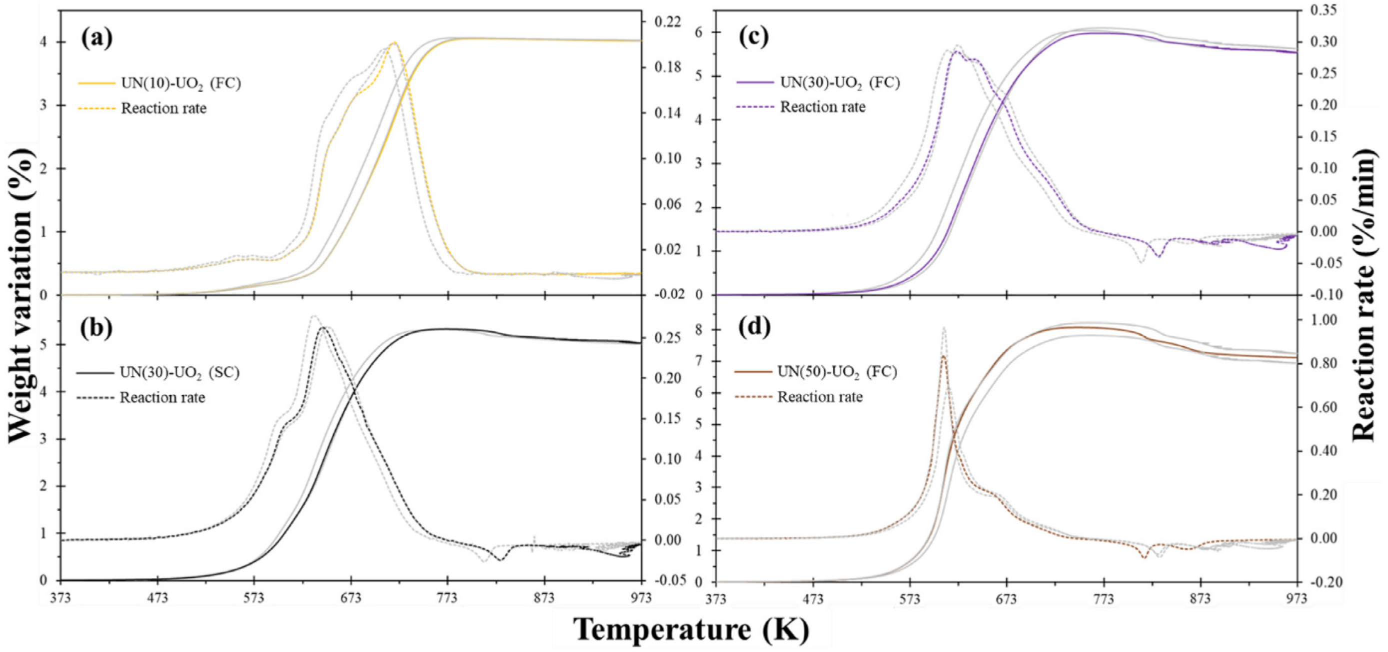

Fig. A2. Triplicate measurements of (a) UN(10)-UO_2 (FC), (b) UN(30)-UO_2 (SC), (c) UN(30)-UO_2 (FC), and (d) UN(50)-UO_2 (FC). The coloured/bolded curves are the ones used in the article. The results show good repeatability and reliability of the TGA experiments.

References

[1] M. Pellegrini, K. Dolganov, L.E. Herranz, H. Bonneville, D. Luxat, M. Sonnenkalb, J. Ishikawa, J.H. Song, R.O. Gauntt, L.F. Moguel, F. Payot, Y. Nishi, Benchmark study of the accident at the Fukushima Daiichi NPS: best-estimate case, Nucl. Technol. 196 (2016) 198–210 https://doi.org/10.13182/NT16-63.

[2] B.R. Sehgal, Light water reactor safety: a historical review, Nuclear Safety in Light Water Reactors, Chapter 1 (2012) 1–88 http://dx.doi.org/10.1016/B978-0-12-388446-6.00001-0.

[3] P.E. Evans, T.J. Davies, Uranium nitrides, J. Nucl. Mater. 10 (l963) 43-55, DOI: https://doi.org/10.1016/0022-3115(63)90115-6.

[4] J. Zakova, J. Wallenius, Fuel residence time in BWRs with nitride fuels, Ann. Nucl. Energy 47 (2012) 182–191 https://doi.org/10.1016/j.anucene.2012.03.033.

[5] G.J. Youinou, R.S. Sen, Impact of accident-tolerant fuels and claddings on the overall fuel cycle: a preliminary systems analysis, Nucl. Technol. 188 (2014) 123–138 https://doi.org/10.13182/NT14-22.

[6] H. Zhao, D. Zhu, K.S. Chaudri, S. Qiu, W. Tian, G. Su, Preliminary transient thermal-hydraulic analysis for new coated UN and UC fuel options in SCWR, Prog. Nucl. Energy 71 (2014) 152–159 https://doi.org/10.1016/j.pnucene.2013.11.008.

[7] G.A. Rama Rao, S.K. Mukerjee, V.N. Vaidya, V. Venugopal, D.D. Sood, Oxidation and hydrolysis kinetic studies on UN, J. Nucl. Mater. 185 (1991) 231–241 https://doi.org/10.1016/0022-3115(91)90340-D.

[8] P.A. Lessing, Oxidation protection of uranium nitride fuel using liquid phase sintering, INL/EXT-12-24974, technical report, 2012, INL, DOI: http://doi.org/10.2172/1036778.

[9] P. Malkki, Licentiate thesis, KTH Royal Institute of Technology, Stockholm, Sweden, 2015.

[10] K.D. Johnson, A.M. Raftery, D.A. Lopes, J. Wallenius, Fabrication and microstructural analysis of UN-U_3Si_2 composites for accident tolerant fuel applications, J. Nucl. Mater. 477 (2016) 18–23 https://doi.org/10.1016/j.jnucmat.2016.05.004.

[11] L.H. Ortega, B.J. Blamer, J.A. Evans, S.M. McDeavitt, Development of an accident-tolerant fuel composite from uranium mononitride (UN) and uranium sesquisilicide (U_3Si_2) with increased uranium loading, J. Nucl. Mater. 471 (2016) 116–121 https://doi.org/10.1016/j.jnucmat.2016.01.014.

[12] B.J. Jaques, J. Watkins, J.R. Croteau, G.A. Alanko, B. Tyburska-Püschel, M. Meyer, P. Xu, E.J. Lahoda, D.P. Butt, Synthesis and sintering of UN-UO_2 fuel composites, J. Nucl. Mater. 466 (2015) 745–754 https://doi.org/10.1016/j.jnucmat.2015.06.029.

[13] J.H. Yang, D.-J. Kim, K.S. Kim, Y.-H. Koo, UO_2-UN composites with enhanced uranium density and thermal conductivity, J. Nucl. Mater. 465 (2015) 509–515 https://doi.org/10.1016/j.jnucmat.2015.06.039.

[14] Y. Mishchenko, Master thesis in Nuclear Energy Engineering, KTH Royal Institute of Technology, Stockholm, Sweden, 2018.

[15] R.M. Dell, V.J. Wheeler, The ignition of uranium mononitride and uranium monocarbide in oxygen, J. Nucl. Mater. 21 (1967) 328–336 https://doi.org/10.1016/0022-3115(67)90185-7.

[16] R.M. Dell, V.J. Wheeler, N.J. Bridger, Hydrolysis of uranium mononitride, Trans. Faraday Soc. 63 (1967) 1286–1294 https://doi.org/10.1039/TF9676301286.

[17] M. Paljević, Z. Despotović, Oxidation of uranium mononitride, J. Nucl. Mater. 57 (1975) 253–257 https://doi.org/10.1016/0022-3115(75)90208-1.

[18] G.W.C. Silva, C.B. Yeamans, A.P. Sattelberger, T. Hartmann, G.S. Cerefice, K.R. Czerwinski, Reaction sequence and kinetics of uranium nitride decomposition, Inorg. Chem 48 (2009) 10642 http://doi.org/10.1021/ic901165j.

[19] L. Lu, F. Li, Y. Hu, H. Xiao, B. Bai, Y. Zhang, L. Luo, J. Liu, K. Liu, The initial oxidation behaviors of uranium nitride UN_x ($x = 0$, 0.23, 0.68, 1.66) films, J. Nucl. Mater. 480 (2016) 189–194 https://doi.org/10.1016/j.jnucmat.2016.08.025.

[20] K. Johnson, V. Ström, J. Wallenius, D.A. Lopes, Oxidation of accident tolerant fuel candidates, J. Nucl. Sci. Technol. 54 (2017) 280–286 http://doi.org/10.1080/00223131.2016.1262297.

[21] D.A. Lopes, S. Uygur, K. Johnson, Degradation of UN and UN-U_3Si_2 pellets in steam environment, J. Nucl. Sci. Technol. 54 (2017) 405–413 http://doi.org/10.1080/00223131.2016.1274689.

[22] M. Jolkkonen, P. Malkki, K. Johnson, J. Wallenius, Uranium nitride fuels in superheated steam, J. Nucl. Sci. Technol. 54 (2017) 513–519, doi:10.1080/00223131.2017.1291372.

[23] H. Li, H. Zhong, Y. Gu, G. Zhang, G. Li, Y. Zhang, P. Zhou, Y. Hu, K. Liu, Oxidation kinetics of nitrided uranium determined by ultraviolet-visible reflectance spectroscopy, J. Alloys Compd 763 (2018) 153–158 https://doi.org/10.1016/j.jallcom.2018.05.187.

[24] L. Luo, Y. Hu, Q. Pan, Z. Long, L. Lu, K. Liu, X. Wang, Extended study on oxidation behaviors of $UN_{0.68}$ and $UN_{1.66}$ by XPS, J. Nucl. Mater. 501 (2018) 371–380 https://doi.org/10.1016/j.jnucmat.2018.01.020.

[25] J.K. Watkins, D.P. Butt, B.J. Jaques, Microstructural degradation of UN and UN-UO_2 composites in hydrothermal oxidation conditions, J. Nucl. Mater. 518 (2019) 30–40 https://doi.org/10.1016/j.jnucmat.2019.02.027.

[26] E.L. Bright, S. Rennie, A. Siberry, K. Samani, K. Clarke, D.T. Goddard, R. Springell, Comparing the corrosion of uranium nitride and uranium dioxide surfaces with H_2O_2, J. Nucl. Mater. 518 (2019) 202–207 https://doi.org/10.1016/j.jnucmat.2019.03.006.

[27] A.P. Shivprasad, A. C. Telles, J. T. White, Report on waterproofing of UN studies, LA-UR-19-28422, Nuclear Technology Research and Development, 2019, Los Alamos National Laboratory, DOI: https://doi.org/10.2172/1565797.

[28] D.R. Costa, M. Hedberg, S.C. Middleburgh, J. Wallenius, P. Olsson, D.A. Lopes, UN microspheres embedded in UO_2 matrix: an innovative accident tolerant fuel, J. Nucl. Mater. 540 (2020) 152355 https://doi.org/10.1016/j.jnucmat.2020.152355.

[29] K. Une, K. Nogita, S. Kashibe, M. Imamura, Microstructural change and its influence on fission gas release in high burnup UO_2 fuel, J. Nucl. Mater. 188 (1992) 65–72 https://doi.org/10.1016/0022-3115(92)90455-T.

[30] A.R. Massih, UO2 fuel oxidation and fission gas release, Report number: 2018:25, SSM (Swedish Radiation Safety Authority), 2018, Sweden, ISSN: 2000-0456, available on: https://www.stralsakerhetsmyndigheten.se/contentassets/f52c9deecaf4441194fa8220d829b040/201825-uo2-fuel-oxidation-and-fission-gas-release.pdf.

[31] C. Ekberg, D.R. Costa, M. Hedberg, M. Jolkkonen, Nitride fuel for Gen IV nuclear power systems, J. Radioanalyt. Nucl. Chem. (2018) https://doi.org/10.1007/s10967-018-6316-0.

[32] L.G. Gonzalez Fonseca, M. Hedberg, L. Huan, P. Olsson, T. Retegan Vollmer, Application of SPS in the fabrication of UN and (U,Th)N pellets from microspheres, J. Nucl. Mater. 536 (2020) 152181 https://doi.org/10.1016/j.jnucmat.2020.152181.

[33] O. Guillon, J. Gonzalez-Julian, B. Dargatz, T. Kessel, G. Schierning, J. Räthel, M. Herrmann, Field-assisted sintering technology/spark plasma sintering: mechanisms, materials, and technology developments, Adv. Eng. Mater. (2014) https://doi.org/10.1002/adem.201300409.

[34] P. Cavaliere, Spark plasma sintering of materials: advances in processing and applications, Springer Nature, Switzerland, 2019 https://doi.org/10.1007/978-3-030-05327-7.

[35] R.A. Johnson, I. Miller, J.E. Freund,), Miller & Freund's Probability and Statistics for Engineers, nineth ed., Pearson Education, London, 2016 ISBN: 978-0321986245.

[36] K.D. Johnson, J. Wallenius, M. Jolkkonen, A. Claisse, Spark plasma sintering and porosity studies of uranium nitride, J. Nucl. Mater. 473 (2016) 13–17 https://doi.org/10.1016/j.jnucmat.2016.01.037.

[37] L. Lutterotti, M. Bortolotti, G. Ischia, I. Lonardelli, H.-R. Wenk, Rietveld texture analysis from diffraction images, Z. Krist. (Suppl. 26) (2007) 125–130 https://doi.org/10.1524/9783486992540-020.

[38] L. Lutterotti, MAUD tutorial - instrumental broadening determination, Dipartimento di Ingegneria dei Materiali, Università di Trento, 2006 online available on: http://www.ing.unitn.it/~maud/tutorial/InstrumentalBroadening.pdf .

[39] R.E. Rundle, A.S. Wilson, N.C. Baenziger, R.A. McDonald, The structures of the carbides, nitrides and oxides of uranium, J. Am. Chem. Soc. 70 (1948) 99–105 https://doi.org/10.1021/ja01181a029.

[40] M.D. Abràmoff, P.J. Magalhães, S.J. Ram, Image processing with ImageJ, Biophotonics Internation 11 (2004) 36–42 available on: https://imagescience.org/meijering/publications/download/bio2004.pdf .

[41] T. Ferreira, W.S. Rasband, ImageJ user guide - IJ 1.46, (2010–2012), available on: http://imagej.nih.gov/ij/docs/guide/.

[42] M.-C. Lee, C.-J. Wu, Conversion of UF_6 to UO_2: a quasi-optimization of the ammonium uranyl carbonate process, J. Nucl. Mater. 185 (1991) 190–201 https://doi.org/10.1016/0022-3115(91)90335-5.

[43] F. Grønvold, High-temperature X-ray study of uranium oxides in the UO_2-U_3O_8 region, J. Inorg. Nucl. Chem. 1 (1955) 357–370 https://doi.org/10.1016/0022-1902(55)80046-2.

[44] B.T.M. Willis, Structures of UO_2, UO_{2+x} and U_4O_9 by neutron diffraction, J. Phys 25 (1964) 431–439 https://doi.org/10.1051/jphys:01964002505043100.

[45] L. Hälldahl, Studies of reactions occurring in the AUC-process: from UF6 to sintering UO2 pellets, Doctoral thesis, 1985, Stockholm University, Sweden. ISBN 91-7146-647-9, Series: Chemical communications, 0366-5607;1985:2.

[46] B.D. Cullity, Elements of X-ray diffraction, second ed., Addison-Wesley, United States of America, 1978 ISBN: 0-201-01174-3.

[47] L. Ge, G. Subhasha, R.H. Baney, J.S. Tulenko, Influence of processing parameters on thermal conductivity of uranium dioxide pellets prepared by spark plasma sintering, J. Eur. Ceram. Soc. 34 (2014) 1791–1801 https://doi.org/10.1016/j.jeurceramsoc.2014.01.018.

[48] R.M. Dell, V.J. Wheeler, E.J. McIve, Oxidation of uranium mononitride and uranium monocarbide, Trans. Faraday Soc. 62 (1966) 3591–3606 https://doi.org/10.1039/TF9666203591.

[49] R.M. German, Sintering: from Empirical Observations to Scientific Principles, first ed., Butterworth-Heinemann, Oxford, 2014.

[50] K.D. Johnson, D.A. Lopes, Grain growth in uranium nitride prepared by spark plasma sintering, J. Nucl. Mater. 503 (2018) 75–80 https://doi.org/10.1016/j.jnucmat.2018.02.041.

[51] T.B. Lindemer, Kinetics of the UO_2-C-N_2 reaction at 1700°C, J. Am. Ceram. Soc. 55 (1972) 601–605 https://doi.org/10.1111/j.1151-2916.1972.tb13452.x.

[52] C. Guéneau, M. Baichi, D. Labroche, C. Chatillon, B. Sundmane, Thermodynamic assessment of the uranium-oxygen system, J. Nucl. Mater. 304 (2002) 161–175 https://doi.org/10.1016/S0022-3115(02)00878-4.

[53] J.L. Henry, R. Blickensderfer, The quaternary system U-C-O-N at 1700°C, J. Am. Ceram. Soc. 52 (1969) 534–539 https://doi.org/10.1111/j.1151-2916.1969.tb09159.x.

[54] H. Tagawa, Equilibrium nitrogen pressures and thermodynamic properties of uranium sesquinitride, J. Nucl. Mater. 41 (1971) 313–319 https://doi.org/10.1016/0022-3115(71)90168-1.

[55] T.B. Lindemer, Chemical thermodynamic representation of nonstoichiometry in $UO_{2-x}N_{3x/4}$, CALPHAD 13 (1989) 109–113 https://doi.org/10.1016/0364-5916(89)90011-4.

[56] S.A. Utlak, J.W. McMurray, Thermodynamic modeling of the U_3O_{8-x} solid solution phase, J. Nucl. Mater. 530 (2020) 151844 https://doi.org/10.1016/j.jnucmat.2019.151844.

[57] R.J. McEachern, P. Taylor, A review of the oxidation of uranium dioxide at temperatures below 400°C, J. Nucl. Mater. 254 (1998) 87–121 https://doi.org/10.1016/S0022-3115(97)00343-7.

[58] T.R.G. Kutty, P.V. Hegde, K.B. Khan, U. Basak, S.N. Pillai, A.K. Sengupta, G.C. Jain, S. Majumdar, H.S. Kamath, D.S.C. Purushotham, Densification behaviour of UO_2 in six different atmospheres, J. Nucl. Mater. 305 (2002) 159–168 https://doi.org/10.1016/S0022-3115(02)00934-0.

[59] J. Williams, E. Barnes, R. Scott, A. Hall, Sintering of uranium oxides of composition UO_2 to U_3O_8 in various atmospheres, J. Nucl. Mater. 1 (1959) 28–38 https://doi.org/10.1016/0022-3115(59)90008-X.

[60] I. Greenquist, M.R. Tonks, Y. Zhang, Review of sintering and densification in nuclear fuels: Physical mechanisms, experimental results, and computational models, J. Nucl. Mater. 507 (2018) 381–395 https://doi.org/10.1016/j.jnucmat.2018.03.046.

[61] R.J. McEachern, A review of kinetic data on the rate of U_3O_7 formation on UO_2, J. Nucl. Mater. 245 (1997) 238–247 https://doi.org/10.1016/S0022-3115(96)00733-7.

[62] R.J. McEachern, J.W. Choi, M. Kolár, W. Long, P. Taylor, Determination of the activation energy for the formation of U_3O_8 on UO_2, J. Nucl. Mater. 249 (1997) 58–69 https://doi.org/10.1016/S0022-3115(97)00189-X.

[63] E.J. Lahoda, F.A. Boylan, Development of LWR fuels with enhanced accident tolerance: ATF Feasibility analysis and final technical report deliverable for the Westinghouse accident tolerant fuel program, Technical Report GATFT-19-004, rev. 2 (2019) United States, DOI: http://doi.org/10.2172/1511013.

[64] K.K. Bae, B.G. Kim, Y.W. Lee, M.S. Yang, H.S. Park, Oxidation behavior of unirradiated UO_2 pellets, J. Nucl. Mater. 209 (1994) 274–279 https://doi.org/10.1016/0022-3115(94)90263-1.

[65] F. Valdivieso, V. Francon, F. Byasson, M. Pijolat, A. Feugier, V. Peres, Oxidation behaviour of unirradiated sintered UO_2 pellets and powder at different oxygen partial pressures, above 350°C, J. Nucl. Mater. 354 (2006) 85–93 https://doi.org/10.1016/j.jnucmat.2006.02.096.

[66] G. Ledergerber, Z. Kopajtic, F. Ingold, R.W. Stratton, Preparation of uranium nitride in the form of microspheres, J. Nucl. Mater. 188 (1992) 28–35 https://doi.org/10.1016/0022-3115(92)90450-Y.

[67] C.M. Silva, T.B. Lindemer, S.R. Voit, R.D. Hunt, T.M. Besmann, K.A. Terrani, L.L. Snead, Characteristics of uranium carbonitride microparticles synthesized using different reaction conditions, J. Nucl. Mater. 454 (2014) 405–412 https://doi.org/10.1016/j.jnucmat.2014.08.038.

[68] K.A. Terrani, B.C. Jolly, J.M. Harp, Uranium nitride tristructural-isotropic fuel particle, J. Nucl. Mater 531 (2020) 152034 https://doi.org/10.1016/j.jnucmat.2020.152034.

[69] L. Quémard, L. Desgranges, V. Bouineau, M. Pijolat, G. Baldinozzi, N. Millot, J-C. Nièpce, P. Arnaud, On the origin of the sigmoid shape in the UO_2 oxidation weight gain curves, J. Eur. Ceram. Soc. 29 (2009) 2791–2798 https://doi:10.1016/j.jeurceramsoc.2009.04.010.

[70] P. Taylor, D.D. Wood, A.M. Duclos, The early stages of U_3O_8 formation on unirradiated CANDU UO_2 fuel oxidized in air at 200-300°C, J. Nucl. Mater. 189 (1992) 116–123 https://doi.org/10.1016/0022-3115(92)90425-K.

[71] S. Aronson, R.B. Roof, J. Belle, Kinetic study of the oxidation of uranium dioxide, J. Chem. Phys. 27 (1957) 137–144 https://doi.org/10.1063/1.1743653.